UNIVERSITY OF OKLAHOMA

GRADUATE COLLEGE

# 3D MARINE SEISMIC PROCESSING FOR INTERPRETATION OF THE JEJU BASIN, SOUTH KOREA

A THESIS

SUBMITTED TO THE GRADUATE FACULTY

in partial fulfillment of the requirements for the

Degree of

MASTER OF SCIENCE

By

DALTON WAYNE HAWKINS
Norman, Oklahoma
2013

3D MARINE SEISMIC PROCESSING FOR INTERPRETATION OF THE JEJU BASIN, SOUTH KOREA

A THESIS APPROVED FOR THE
CONOCOPHILLIPS SCHOOL OF GEOLOGY AND GEOPHYSICS

BY

_____
Dr. Kurt J. Marfurt, Chair

_____
Dr. Matthew J. Pranter

_____
Dr. Jamie Rich

For my family, both current and future

## ACKNOWLEDGEMENTS

There are many people to thank for giving me the opportunity to pursue my Master's degree here at the University of Oklahoma along with a long series of events that seem oddly coincidental, if you believe in those sorts of things. First, I would like to thank Dr. Marfurt for being able to take me under his wing and thank my committee members for being patient through my multiple different committees. Also to the late Dr. Tim Kwiatkowski who first introduced me to seismic processing and helped me along the way. When I first came to the University of Oklahoma I was unsure of exactly what aspect of geophysics I wanted to pursue. Fortunately, I learned a great deal here both in and out of the classroom and because of that I have found what I believe to be my true calling.

I must also thank the Korean Institute of Geoscience and Mineral Resources (KIGAM) for providing that data that made this entire project and learning experience possible. Also the Attribute-Assisted Seismic Processing and Interpretation (AASPI) consortium and team members that have created the software and support group that were vital to the success of this project.

The software support that we have here at the University of Oklahoma is fantastic and I would like to thank Halliburton for the ProMAX licenses. It was a tremendous help for processing the data. Furthermore I want to thank Schlumberger for the many Petrel license allowed for the interpretation of the data in a much more convenient manner, and also provided me the enlightening opportunity to teach the software to undergraduate students.

Thanks goes to my fellow colleagues here at the university; especially Alfredo Fernandez and Gabriel Mattei who were there every struggle along the way providing support, assistance and sparking new ideas. A large thanks to Ben Dowdell for merging the raw data into a SEG-Y file with all coordinate information included. Oswaldo Davogustto, Mark Aisenberg, Sumit Verma, and Shiguang Gou for the assistance with the software used to reach the final product.

No department would be complete without amazing management and bureaucratic tape cutters; therefore, I must thank the ever hard working office personnel, Jocelyn Cook, Adrianne Fox, Teresa Hackney, Nancy Leonard, and most certainly Donna Mullins for helping me through the paper struggles.

I would like to thank my family for always being there, and supporting me throughout my entire collegiate career. You provided me the opportunity and tools with which to succeed, and for that I will always be grateful.

Lastly, I would like to thank the good Lord upstairs for helping me through and setting up this most unique, beneficial and challenging experience. I know that without him none of this would have been possible. Philippians 4:10-13 “**10** I rejoiced greatly in the Lord that at last you renewed your concern for me. Indeed, you were concerned, but you had no opportunity to show it. **11** I am not saying this because I am in need, for I have learned to be content whatever the circumstances. **12** I know what it is to be in need, and I know what it is to have plenty. I have learned the secret of being content in any and every situation, whether well fed or hungry, whether living in plenty or in want. **13** I can do all this through him who gives me strength.”

## TABLE OF CONTENTS

## LIST OF TABLES

## LIST OF FIGURES

## ABSTRACT

This work describes the processing, seismic attribute analysis and interpretation of the first non-proprietary 3D marine seismic survey collected over the Jeju Basin in the northern East China Sea. The data were collected by the Korean Institute of Geoscience and Mineral Resources (KIGAM) in June of 2012 and licensed for research use to the University of Oklahoma. The data are of high quality but suffer from strong water bottom multiples. The data were processed using commercial software and imaged using an internal OU prestack time migration application.

Once processed to a final stack, the data were whitened and attribute volumes were generated. Subsequent interpretation revealed 3 of the 4 reported megasequences (MS) along with complex structural deformation including normal faults, conjugate normal faults and rollover anticlines. Investigation within the MS's revealed MS4 to be separated into two distinct portions. The lower portion is interpreted to be non-marine and the upper portion representing the present day marine environment. MS3 contained multiple fluvial systems along with a high amplitude reflector consistent with igneous flows that occurred during this time. Finally, the oldest MS1-2 displayed the highest dips, highest offsets along faults, and growth fault syndepostional features, as well as some interesting high amplitude anomalies interpreted to be the most probable location for hydrocarbon accumulations.

# INTRODUCTION

Occupying an area of approximately 770,000 $km^2$ (297,298 $mi^2$), the East China Sea (ECS) has remained fairly unexplored, with much of the existing data being proprietary. Most studies in the East China Sea utilize 2D seismic data and well data that has been collected by oil and service companies from the 1970's to the 1990's. Since exploration first began in the 1970's many oil and gas fields have been found in the southern portions of the East China Sea and have created political unrest between China and Japan with each claiming the hydrocarbons fall within their territorial boundaries.

While Japan and China dispute over ownership in the southern portions of the East China Sea, Japan and South Korea have reached an amical agreement in the less explored northern portions of the East China Sea to help meet their energy demands. South Korea currently has only one producing field, the Donghae-1 field, in the Ulleung Basin, Korean East Sea (also known as the Sea of Japan) that produces primarily gas. The recent definition of the international boundary between Japan and South Korea has opened northern potions of the East China Sea to South Korea for exploration and possible economic development, specifically the Jeju Basin.

The East China Sea is a large basin lying on the continental margin of Southeast Asia that is broken up into several subbasins by the Guanyin, Haijiao, Hupijiao and Yushan rises (Figure 1). These basement highs separate multiple basins, some of which have been evaluated for hydrocarbon exploration since

the 1970's. The Jeju Basin is located just to the south of the Korean Peninsula, past Jeju Island, and is divided from the greater ECS Basin by the Hupijiao Rise (Figure 1). Several oil and gas fields of Eocene to Oligocene age (Lee et al., 2006) have been found in the southern portions of the East China Sea. Since the formation of all of the sub-basins in the region was contemporaneous, the potential for hydrocarbon formation and collection in the northern parts of the East China Sea is favorable.

Basin analysis by Lee et al. (2006) and Cukur et al. (2012) evaluated source rock, maturity, trap, and seismic hydrocarbon indicators within the Jeju Basin. Potential source rocks include lacustrine facies, fluvial shales and numerous thin coal beds (Lee et al., 2006). Since the ages of these rocks are younger than the Late Cretaceous, maturity and timing of hydrocarbon formation is considered to be the highest risk.

Recently, hydrocarbon reservoirs have been found associated with igneous bodies that are Mesozoic to Cenezoic in age within the rift basins of Eastern China (Cukur et al., 2010, Zhang et al., 2011). Many of the initial 2D seismic lines in the Jeju Basin had bright spots that were thought to be direct hydrocarbon indicators; however, when drilled they were found to be igneous sills. Cukur al. (2010) examined the igneous activity in the Jeju Basin, and found bodies of varying shape and ages. The presence of these igneous intrusions not only affects the maturation of hydrocarbons but can form traps and reservoirs (Farooqui et al., 2009). Basin modeling based on the JDZ-VII-1 well in the deeper southwest part of the Jeju Basin indicates oil formation beginning around 40

m.y.a. and gas formation about 11 m.y.a. (Cukur et al., 2012). Unfortunately, these times mean that the oil maturation window predates the uplift that formed many of the traps.

Because igneous bodies are key in estimating maturation, reservoir, seal, and potential drilling hazards, a major objective is to distinguish igneous intrusives from other facies. Using older Jeju Basin 2D data, Pigott et al. (2013) used seismic attributes to identify both igneous bodies and fluvial features in the basin. In this work, modern 3D processing work flows to the new KIGAM acquired 3D dataset to maximize vertical and lateral resolution was completed. Then 3D seismic attributes and principles of seismic geomorphology delineate potential stratigraphic and structural traps in the basin.

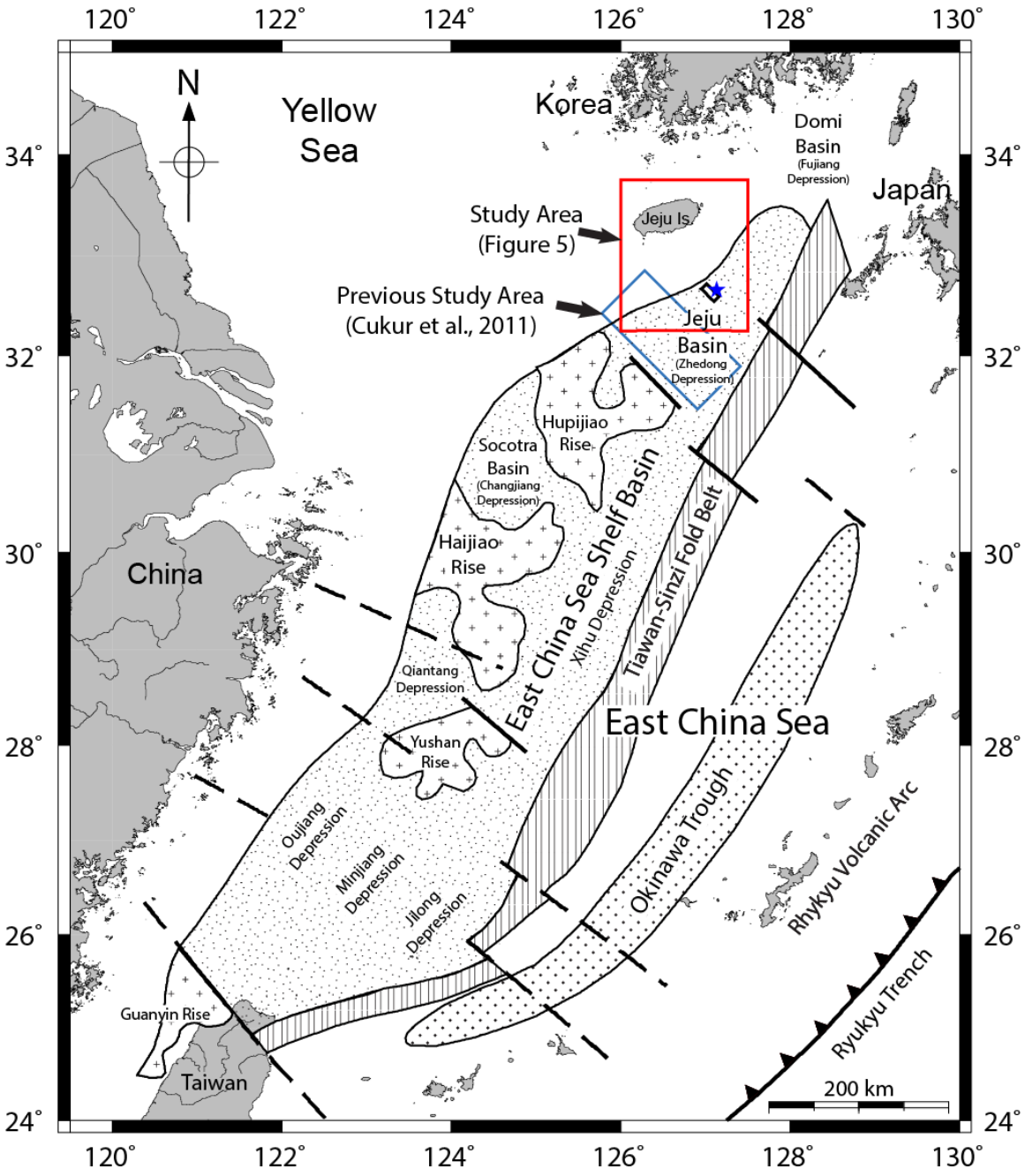


**Figure 1.** Regional map of the East China Sea and its major geologic structural providences. (Modified after Cukur et al., 2011)

## GEOLOGIC SETTING

The East China Sea has been an area of economic interest for exploration and production of hydrocarbons for many years, with both well logs and multichannel seismic reflection profiles. Some of these data cover the Jeju (sometimes written as the Cheju) Basin and have been used to create a stratigraphic and tectonic frame work for the basin. The Jeju Basin is located off the southern coast of the Korean peninsula, past Jeju Island, and is bounded by the Hupijiao Rise to the south and west, the Domi Basin to the northeast, the Taiwan-Sinzi fold belt to the southeast and the Korean Uplift to the northwest (Kwon et al., 2002). This portion of the East China Sea is characterized by small basins, basement highs and basement faults trending NNE. In the northwestern portions of the Jeju Basin, the acoustic basement lies at a depth less than 500 m to 1,500 m and reaches a maximum depth of 5,500 m in the southern portions of the basin (Cukur et al., 2011).

The formation of the Jeju Basin has multiple stages of development, each separated by a period of uplift or inversion: rift phase 1, rift phase 2, post-rift phase 1 and post-rift phase 2 (Cukur et al., 2011). In the Late Cretaceous to the Late Eocene-Early Oligocene, the initial rift phase began, creating the NE trending graben, half-graben basins, and SW dipping faults that characterize much of the northern East China Sea. Rift phase 1 is believed to have begun due to slab roll-back as the Pacific plate slowed its subduction beneath the Eurasian Plate and is the largest stage of extension of the four rift phases with an estimated 2-6.5% of extension, with the most extension occurring in the deeper

southeastern portions of the basin (Cukur et al., 2011). This rift phase was interrupted by the Yuquan Movement resulting from the collision of the Indian and Eurasian plates (Cukur et al., 2011) and creating the Taiwan-Sinzi fold belt to the east (Lee et al., 2006). Rift phase 2 began in the Early Oligocene, shortly after the Yuquan Movement, and continued into the Early Miocene, but at a much smaller magnitude, suggesting that it may be related to deeper tectonic activity and thinning of the lithosphere (Cukur et al., 2011). The second rift phase resulted in approximately 0.7-0.8% extension. A second phase of uplift halted rifting phase 2, but did not result in significant erosion within the Jeju Basin.

The post-rift phases are characterized by regional subsidence and do not continue extension within the basin. In the Early Miocene, after the short uplift period, the first post-rift phase began and continued until the Late Miocene, creating up to 2,000 m of accommodation space. This was interrupted by an inversion period known as the Longjing Movement, which created a long thrust fold belt that covers the Jeju Basin and continues to the north through the Domi Basin. The Longjing Movement is estimated to have created anywhere from 430-900 m of uplift and 0.2-0.4% shortening in the Jeju Basin and is related to the plate convergence of Taiwan and a subducting arc on the Philippine Sea Plate (Cukur et al., 2011). The inversion created enough uplift to cause erosion of the thrust fold belt it formed leaving an easily recognizable unconformity. The final stage, post-rift phase 2, continued regional subsidence in the Jeju Basin and began in the Late Miocene continuing to present day. Cukur et al. (2011) provide

an excellent reconstruction (Figures 2 and 3) and description of the history of the Jeju and surrounding basins.

Each rift phase created additional accommodation space within the basin and hence the Jeju Basin has four megasequences of strata. The first megasequence (MS1) was deposited during the first rift phase during the late Cretaceous to Late Eocene-Early Oligocene and is primarily fluviolacustrine in nature. There are some irregular high-amplitude reflections in the lower portions of MS1 that most likely represent volcanic flows, which would be consistent with the volcanic activity during the early rifting of the basin (Lee et al., 2006). Faulting extends from the basement into the MS1 along which are wedge-shaped bodies that dip away from the faults. These have been interpreted from 2D seismic to be alluvial or deltaic fans (Lee et al., 2006). Megasequence 2 (MS2) was deposited during rift phase 2 resulting in a much thinner megasequence corresponding to less extension during this period. Faults along with wedge-shaped bodies do continue into MS2 indicating continued extension within the basin. Well logs show it to be very similar to the top of MS1, with primarily fluviolacustrine sandstones and mudstones (Lee et al., 2006). During the first post-rift phase of regional subsidence, the third megasequence (MS3) was deposited, covering the entire basin and concealing the underlying rift and graben topography (Lee et al., 2006). MS3 is dominantly nonmarine with a shallow marine environment transgressing from the southeast to the northwest in the upper strata. MS3 lacks any large mappable faults further supporting that there was little extension in post rift phase 1. The inversion in the Late Miocene flattened the thrust fold belt it

created and eroded a significant amount of MS3.The last megasequence (MS4) formed during the final post-rift phase and can be split into two subunits. The lower unit is characterized by nonmarine deposits and the upper subunit by shallow marine and shelf deposits, similar to the current depositional environment (Lee et al., 2006). Figure 4 (Cukur et al., 2011) gives a very good summary of the tectonics and deposition for the Jeju and surrounding basins.

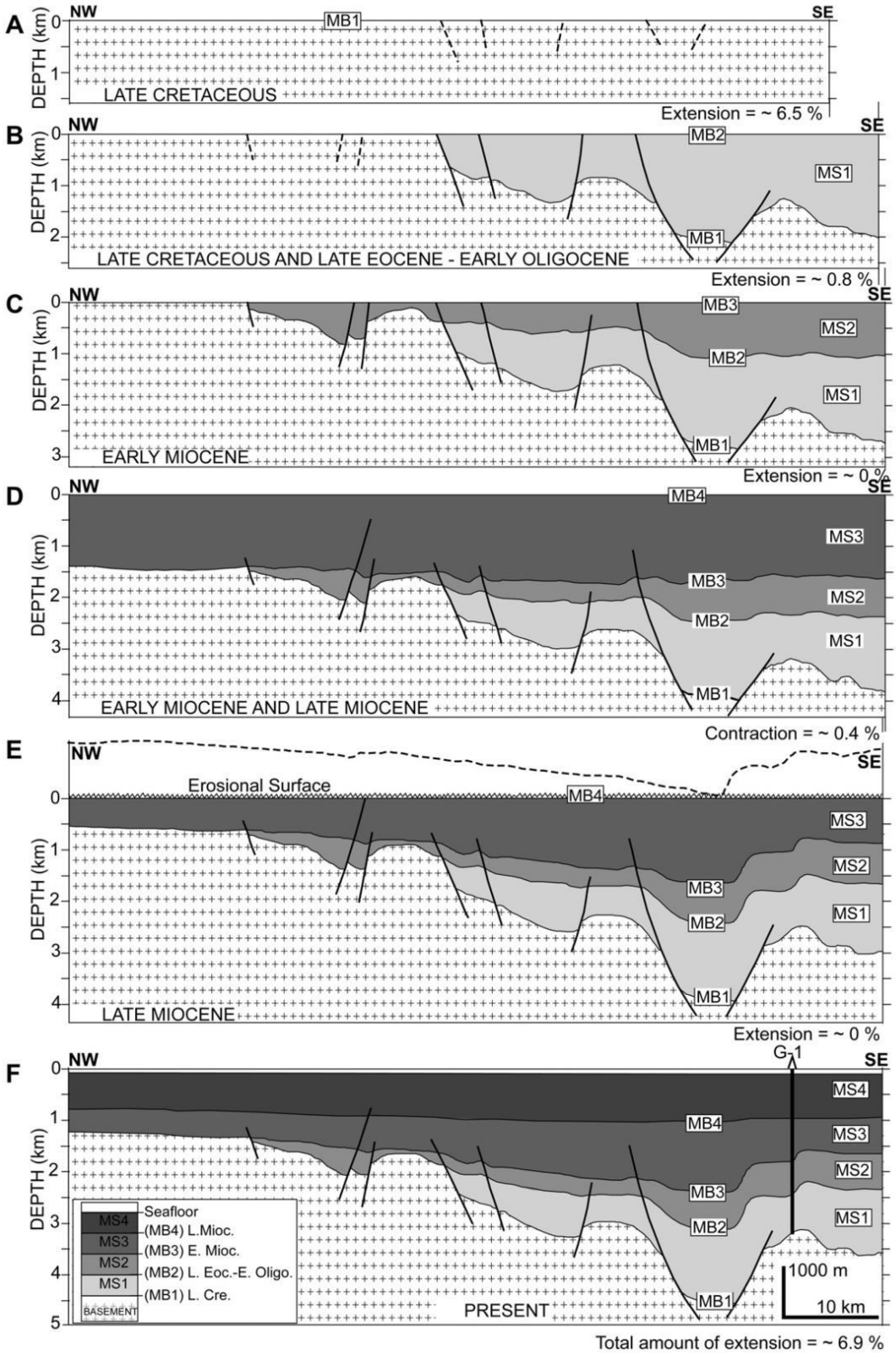


**Figure 2.** Palinspastic reconstruction illustrating the individual rift and uplift stages in the deeper southeastern Jeju Basin. (Cukur et al., 2011)

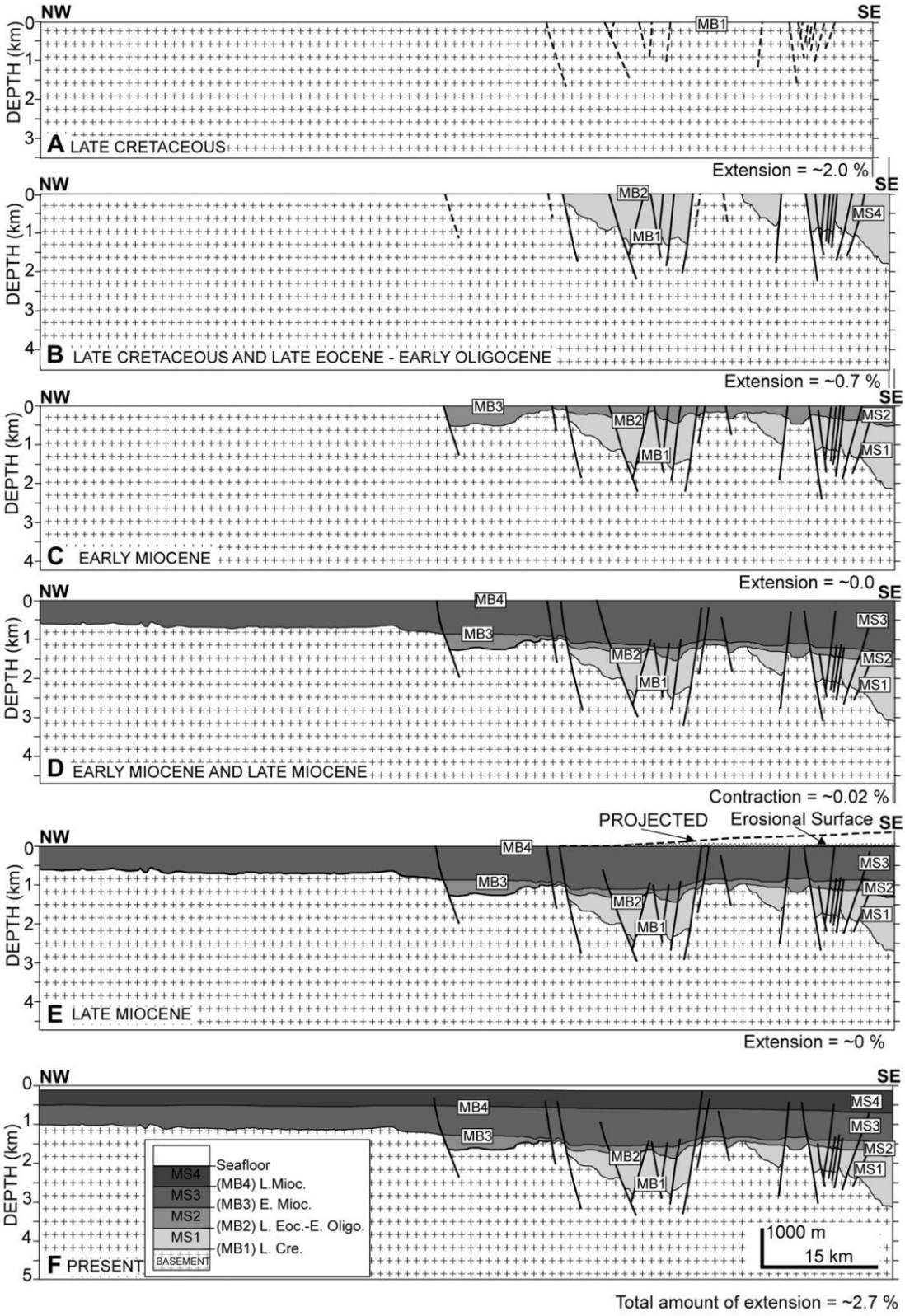


**Figure 3.** Palinspastic reconstruction illustrating the individual rift and uplift stages in the shallower northwestern Jeju Basin (Closer to the study area). (Cukur et al., 2011)

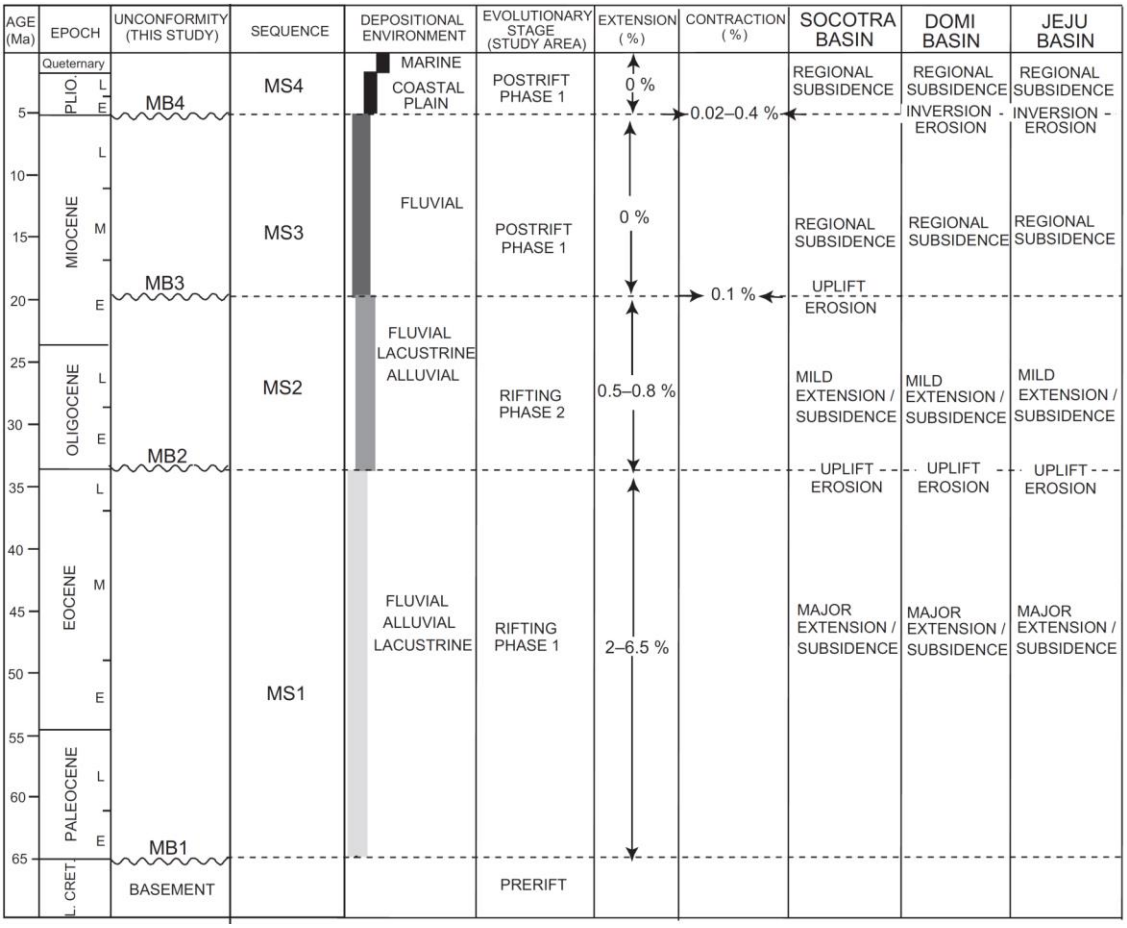


**Figure 4.** Illustration of the structural and stratigraphic evolution of the Jeju and surrounding basins. (Cukur et al., 2011)

# METHODS

## DATA DESCRIPTION

KIGAM provided the 3D data volume in raw SEG-D format with separate files for the coordinate information. The data were acquired in the shallow water (110-150 m) portions of the Jeju Basin located approximately 75 km southeast of Jeju Island (Figure 5). KIGAM is a government institution, somewhat like the U.S. Bureau of Ocean Energy Management (BOEM) or U.S. Geological Survey (USGS) with similar budget constraints. For this reason, the acquisition of the data was designed to be a multiphase campaign extending over several years. Phase 1 was completed by KIGAM through the use of their R/V Tamhae II in June of 2012, with following phases to infill gaps and complete a larger section of the survey. The acquisition comprised of two 2.4 km streamers 100 m apart each with 192 receivers at 12.5 m spacing. Two gun arrays 50 m apart fired alternately every 25 m (each gun fired every 50 m) (Table 1 and Figure 6). With just two streamers and two guns behind the same boat the survey is narrow azimuth, which will come into play in the processing.

The purpose of the survey is to examine the basin as a whole for any potential hydrocarbon resources as well as extend KIGAM's internal 3D marine seismic processing capabilities. Therefore, the processing was done as a general workflow for 3D marine seismic data with no specific exploration target.

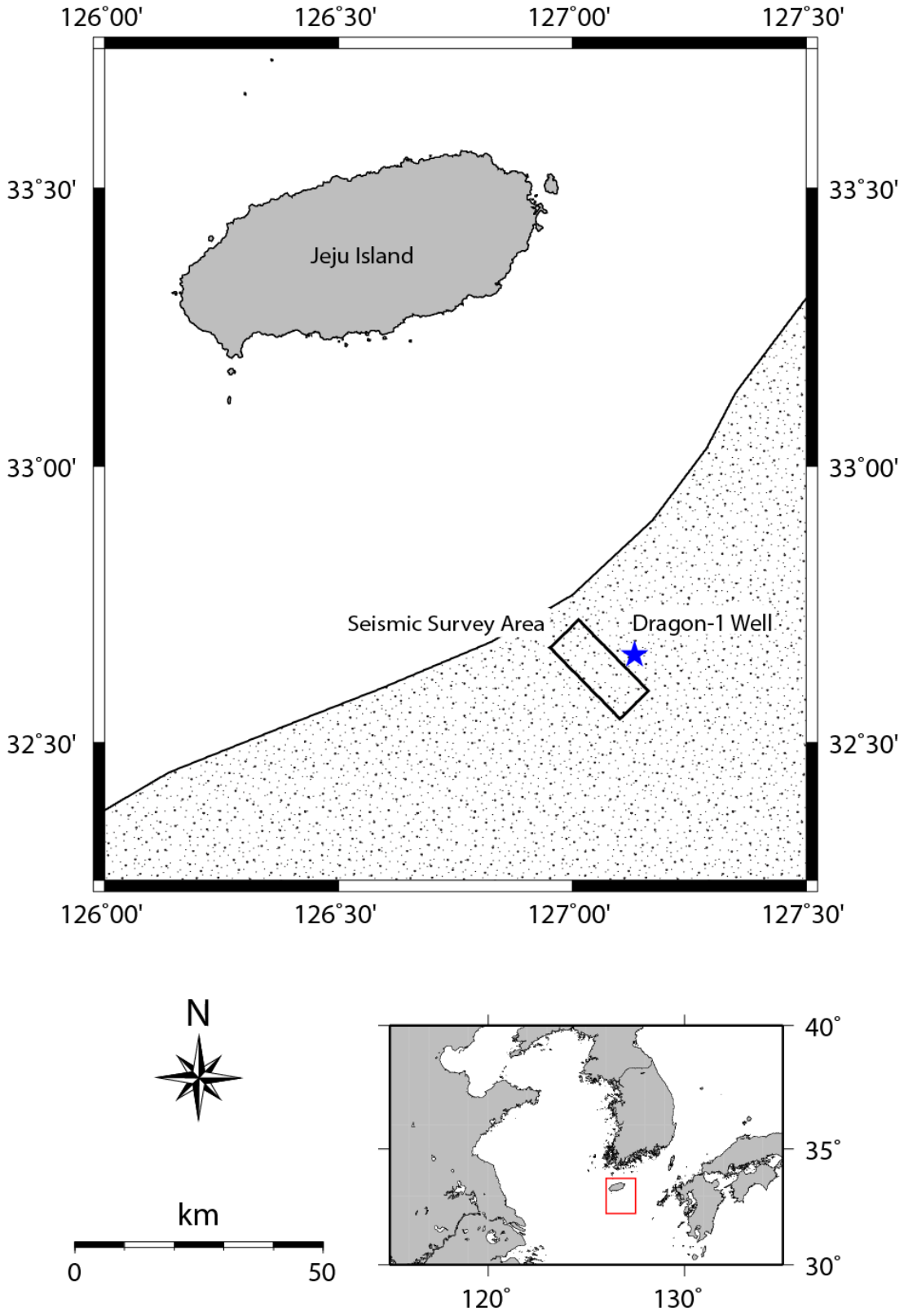


**Figure 5.** Location map illustrating the location of the survey with relation to Jeju Island and the Dragon-1 Well.

| | |
|---|---|
| Number of streamers/airgun arrays | 2/2 |
| Streamer Length/separation | 2.4 km/100 m |
| Streamer/Airgun Depth | 7 m/5 m |
| Number of channels | 192 per streamer |
| Receiver Spacing | 12.5 m |
| Shot spacing | 25 m alternating airguns |
| Source Volume | 1254 $in^3$ |
| Record Length | 5 s (100 ms before shot) |
| Sampling Interval | 2 ms |
| CMP bin size | 25 x 6.25 m |
| Maximum Fold | 92 |
| Average Fold | 24 |

**Table 1.** Summary of seismic acquisition parameters.

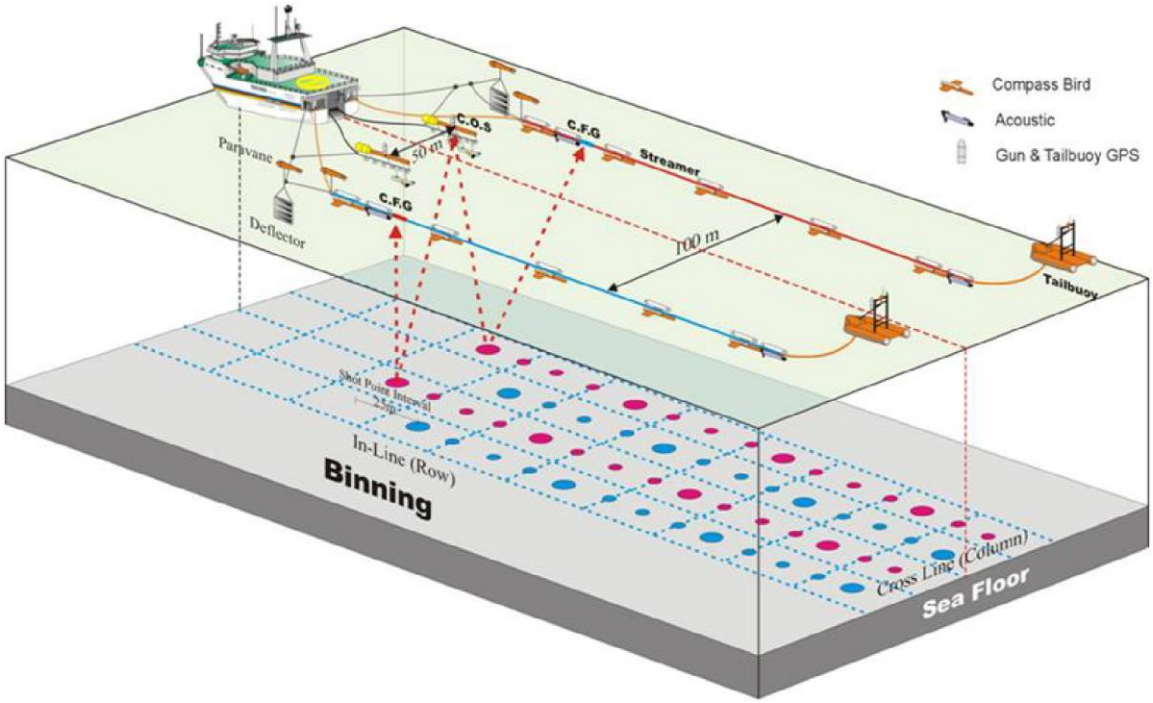


**Figure 6.** Illustration of the seismic acquisition aboard the R/V Tamhae II. (courtesy of KIGAM)

## DATA CONDITIONING

The data were received in its raw SEG-D format with no geometry applied and no coordinates in the headers. Each individual SEG-D was read into ProMAX, a commercial processing package, and the appropriate coordinate files applied to the corresponding SEG-D files. The SEG-D's were then combined into one SEG-Y file with the coordinate information now included. The SEG-Y file was imported into the software and geometry defined with a nominal bin size of 25 x 6.25 m (inline separation by crossline separation) (Figure 7). The next steps included bandpass filtering with corner frequencies 8-15-80-100 Hz (Figure 8), trace editing and common shot spiking deconvolution to minimize the air bubble source wavelet. A quick check of the first arrival times, along with conversations with people present during the acquisition revealed that recording began 100 ms prior to shot initiation requiring removal using a static shift. An initial velocity model was constructed 1 km by 1 km (or 40 x 160 CMP) based on velocity picking on semblance gathers and was used to create a brute stack which revealed severe first and second order water bottom multiples (Figure 9). SRME (surface related multiple elimination) is a completely data driven technique and requires no a priori information to predict the multiples (Verschuur et al., 1992). Although, the dual streamer, narrow azimuth data precluded the use of wide-azimuth SRME, the flat water bottom at 150-110 m gives rise to multiples that are amenable to 2D SRME filtering.

The processing of 3D seismic data through 2D SRME requires a bit of data manipulation. In the software used, SRME requires that you begin with

geometry applied to the shot gathers that have the direct arrival muted. No deconvolution should be performed prior to SRME. Thus, only preconditioning performed here was a top mute, bandpass filter, the 100 ms static shift, and trace header math to define the cable (streamer) number. There are several technical details in running 2D SRME on 3D data volumes. First, one needs to separate the multiple streamers so that each input dataset contains only data from one streamer. Second the data need to be read such that the next shot in the line is in the same direction as the sail direction of the boat collecting the data if this is not the case, the “flip shot direction” needs to be selected (see Appendix A). Figures 10 and 11 show a representative shot gather and stacked line before and after SRME.

SRME removes long period multiples at all offsets but does not compress the source wavelet or remove airbubble effect. To do so one needs to apply deconvolution, true amplitude recovery and trace editing. The deconvolution was done with a 35 ms prediction and 140 ms operator length. True amplitude recovery was done to account for attenuation and geometric spreading with a 1/distance and a 6 dB/s correction down to 3 seconds. Trace editing was performed by running trace statistics then using those statistics to do a trace mute of those traces that lie outside the bell curve. The data were also visually QC’ed by panning through shots at the end and beginning of each shot sequence to check for damaged receivers.

In order to pick a more accurate velocity model, the post SRME data were organized into CMP gathers and subjected to a Radon filter, followed by another

pass of deconvolution. The hyperbolic Radon filter was chosen to help in eliminating deep multiples that remained in the data. The Radon filtered dataset was used only to facilitate velocity picking, beginning with a 30 x 120 CMP grid and ending with a 15 x 60 (or 375 x 375 m) CMP grid. Velocities were picked using 5 crossline by 7 inline supergathers with a 20 ms sampling rate and a 40 ms window. The velocity model was then smoothed across all inlines and crosslines using a small time window to create a velocity trace at each CMP (Figure 12). Figure 13 illustrates the general flow followed in processing the data.

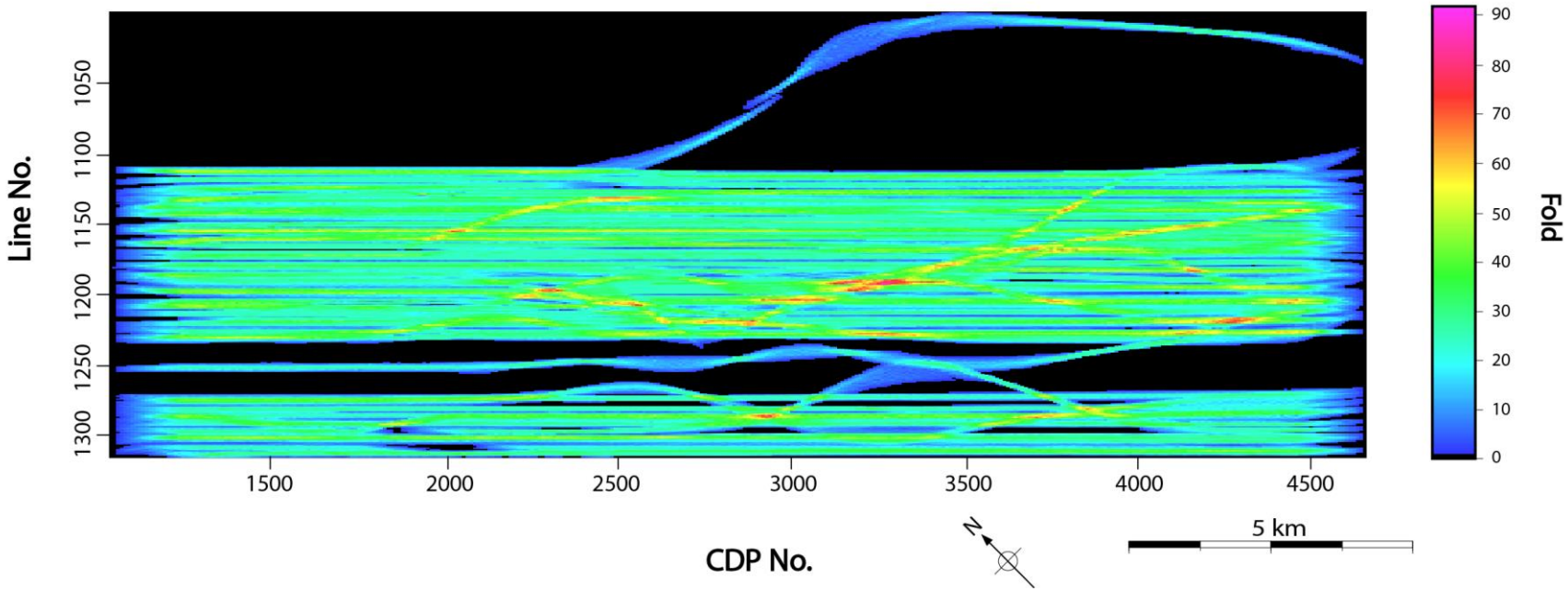


**Figure 7.** Fold map of the survey area. The gap between inlines 1240 and 1275 was due to hardware and weather problems. This gap and data to the northeast encompassing the Dragon 1 well will be acquired during 2013.

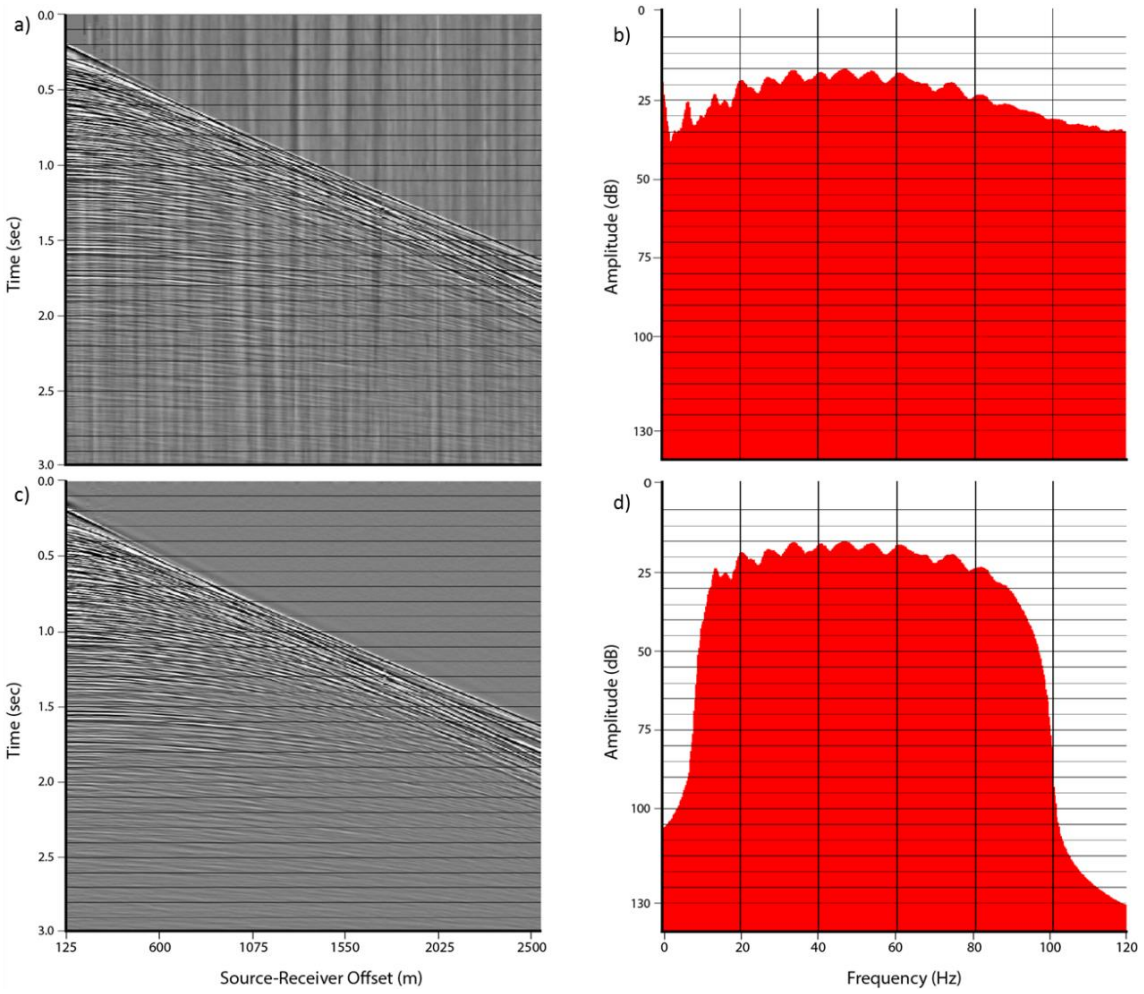


**Figure 8.** (a) A raw shot gather and (b) the raw frequency spectra. (c) The same shot as in (a) after a bandpass filter with corner frequencies at 8-15-80-100. (d) frequency spectra after bandpass filtering.

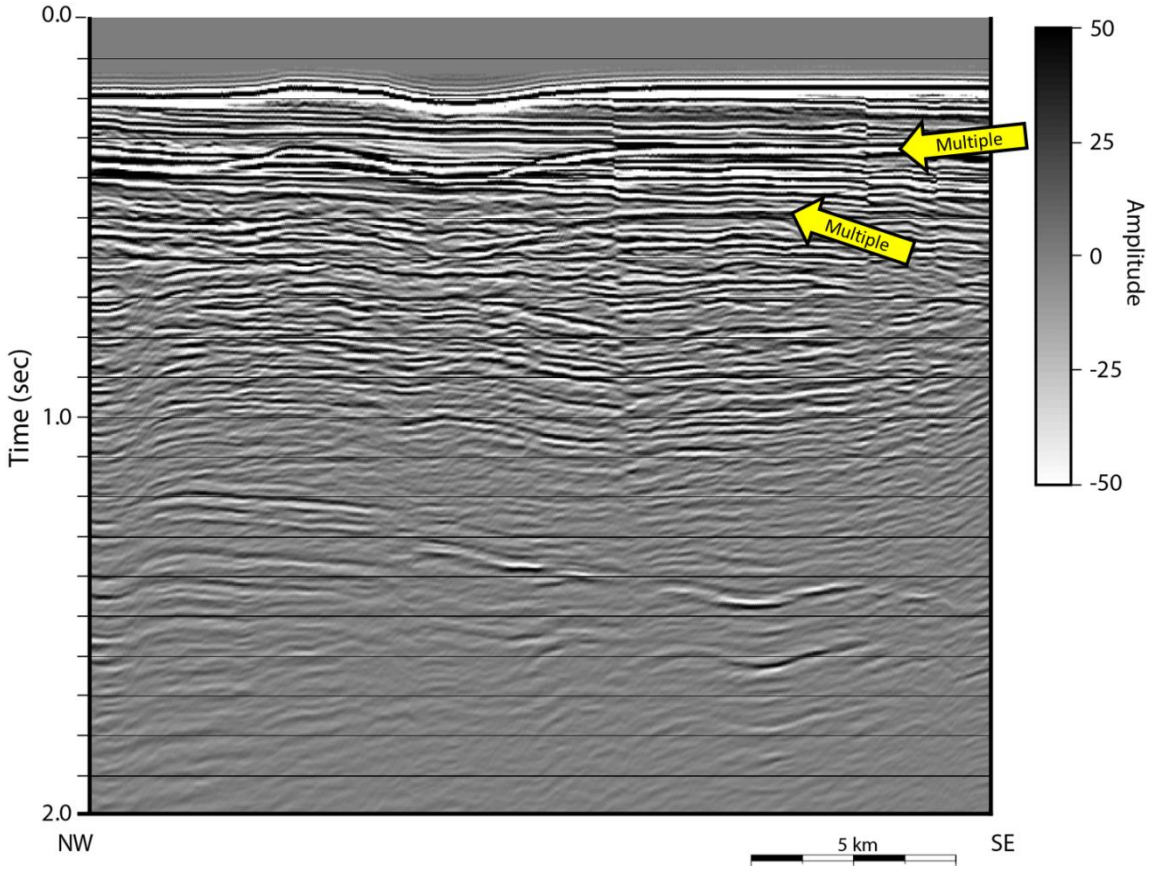


**Figure 9.** Brute stack demonstrating the severe water bottom multiple (yellow arrows) present.

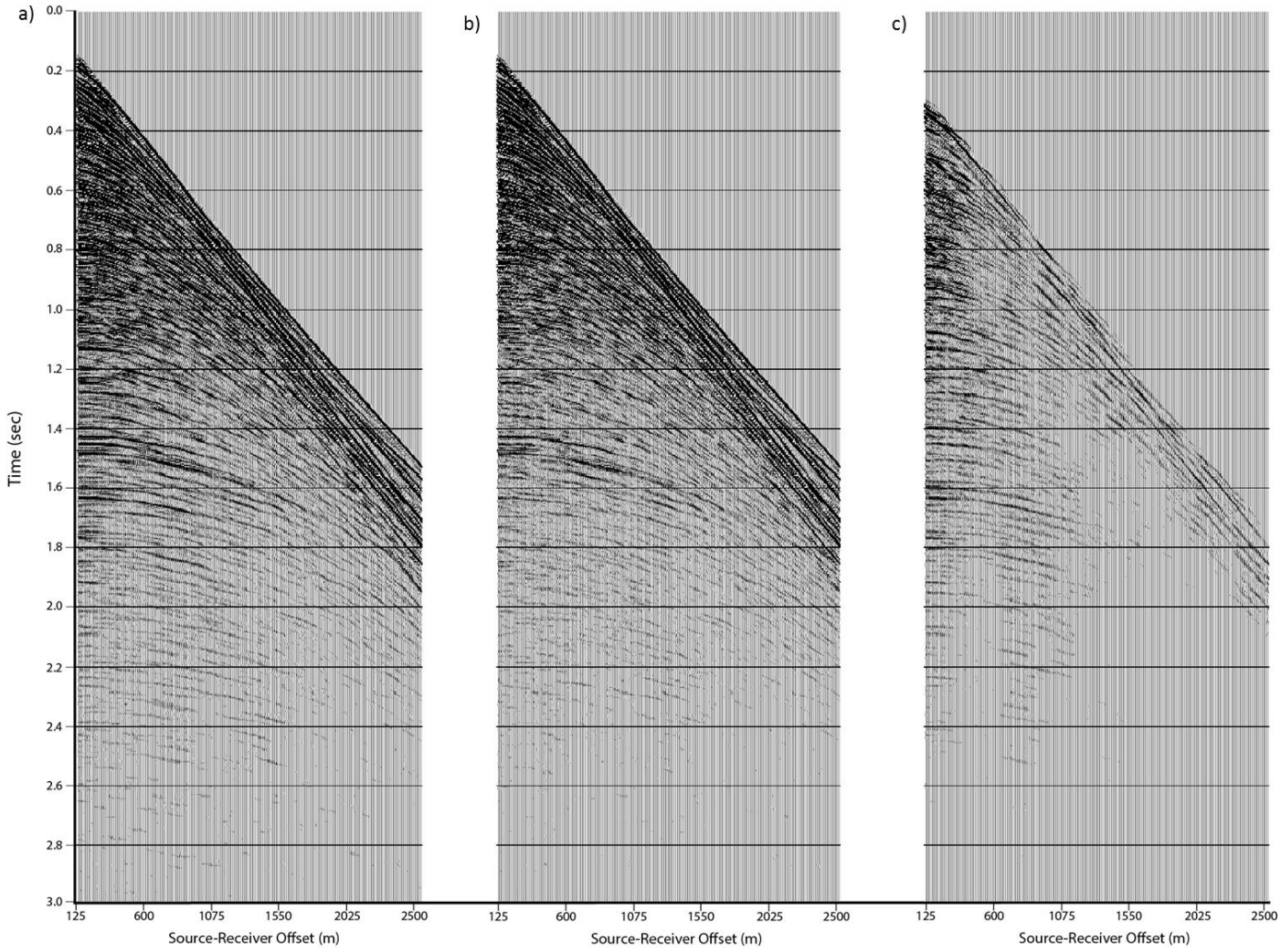


**Figure 10.** Shot gathers (a) before and (b) after SRME. (c) represents the noise removed by SRME. All plots are plotted on the same scale, 4 to -4.

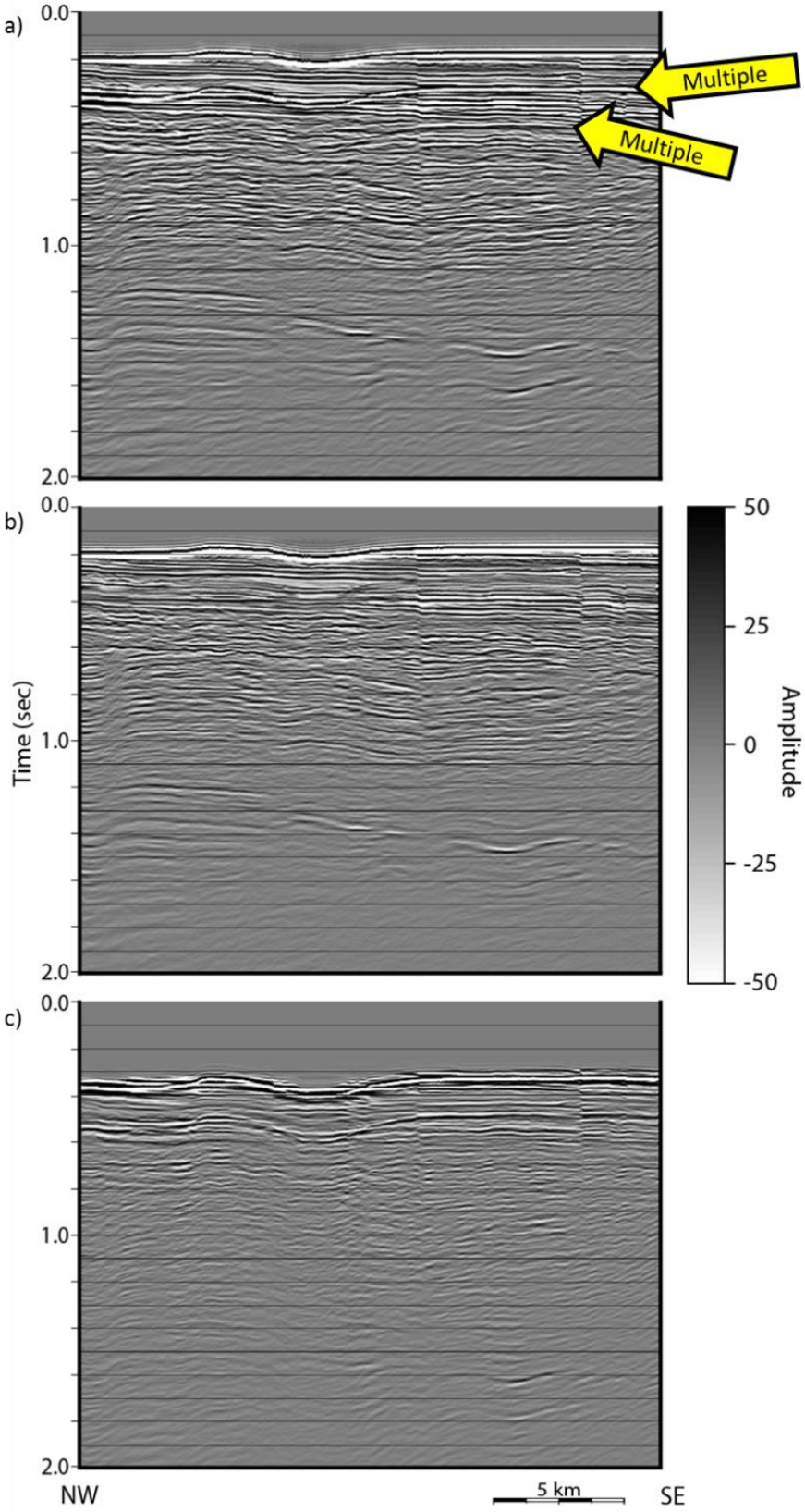


**Figure 11.** (a) stack with the multiples present, (b) stack after SRME and (c) stack of the noise removed.

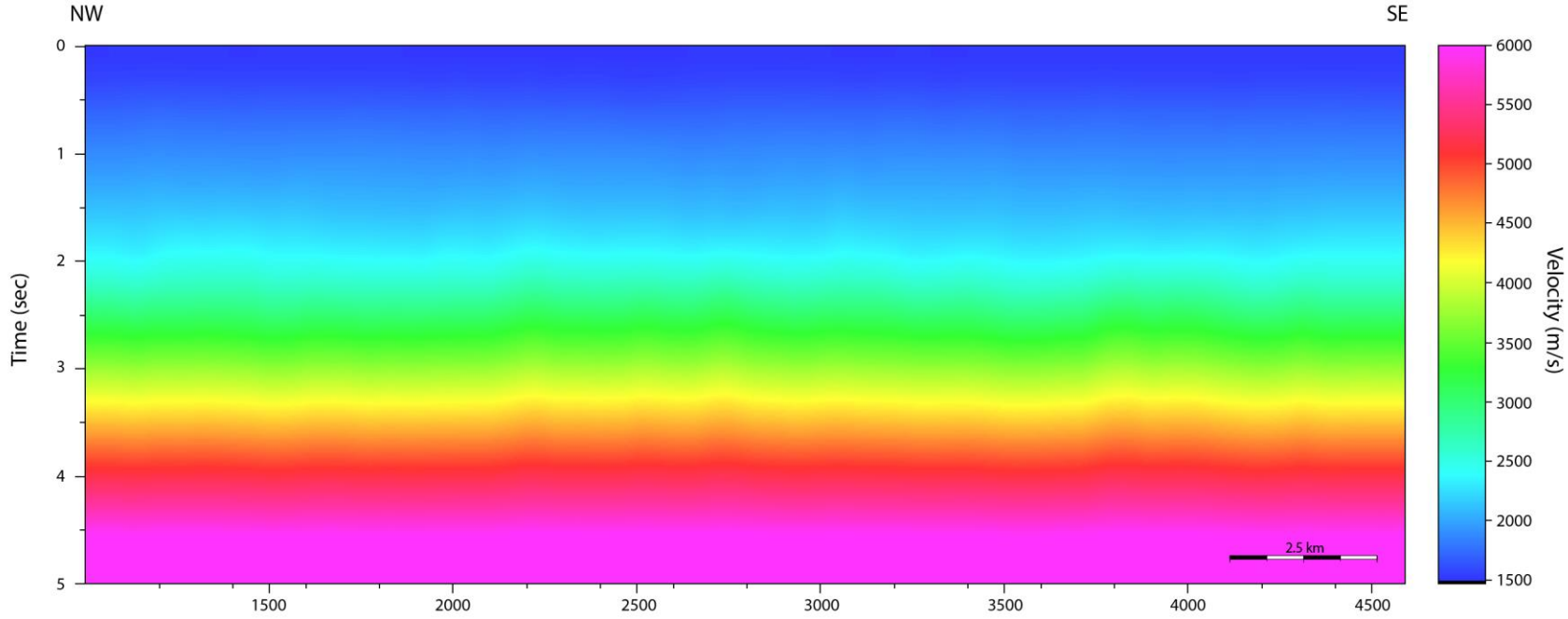


**Figure 12.** Representative line showing the relatively smooth 375 x 375 m velocity grid picked for migration of the data set.

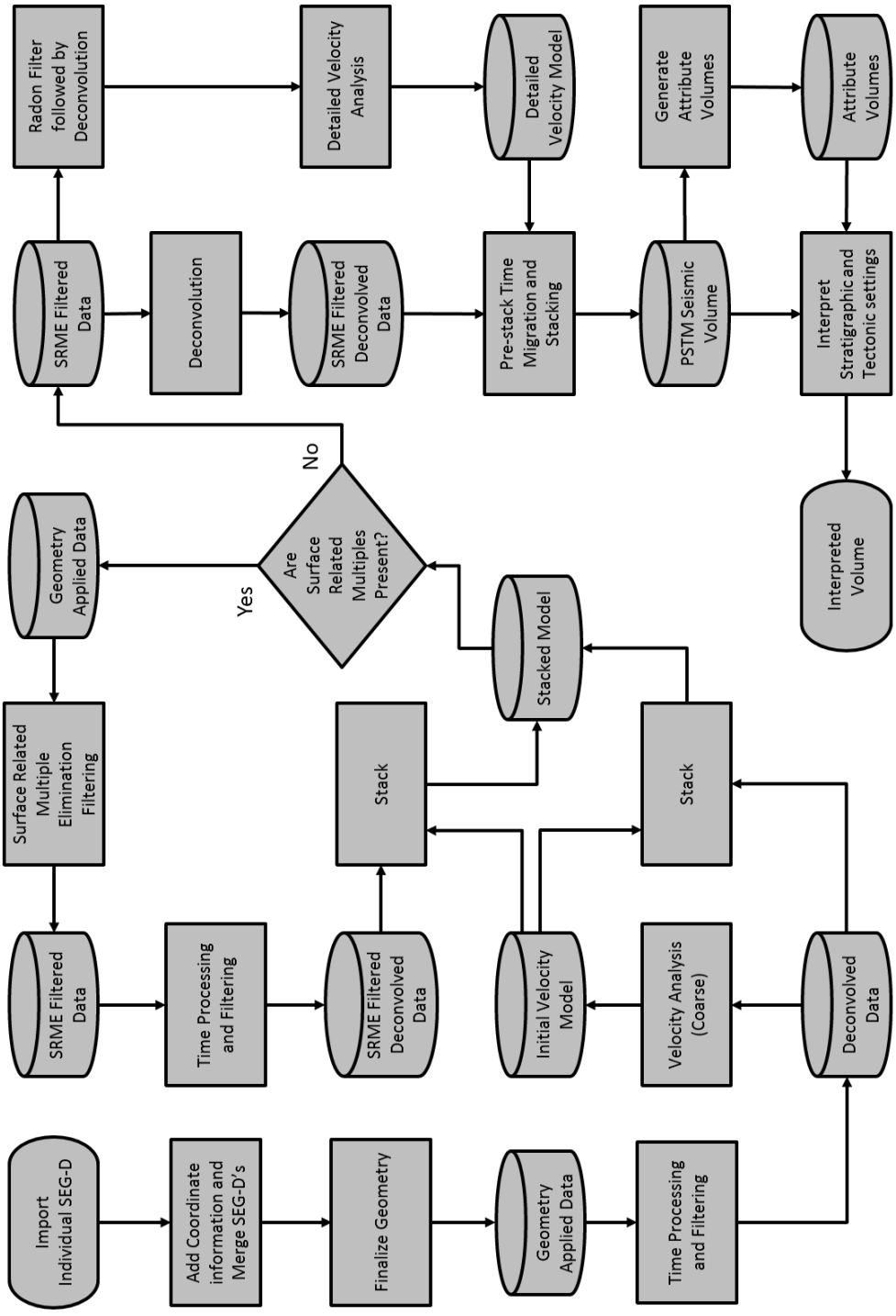


**Figure 13.** General processing flow followed to complete the data processing.

## SEISMIC IMAGING

With the final preconditioned data and the smoothed velocity model in hand the data were prestack time migrated (PSTM) using a Kirchhoff algorithm that generates offset and azimuth lines at each common reflection point (CRP). The data were migrated from 0 to 3 seconds with the smoothed velocity model decimated to 4 ms sampling to reduce the compute time, the input data were sampled at 1 ms (Figure 14). The migration used in this study used 45 offset bins with a maximum offset of 2,569 m, a migration aperture of 5,000 m and only one azimuth, as the survey is very narrow azimuth in nature.

A linear mute of 0.025 (time/offset bin) was then applied to the final migrated gathers to eliminate the stretch noise (Figure 15). The data were then stacked and spectrally whitened using a single time variant function for the entire survey (Figure 16). Upon stacking it became apparent that the data suffered from a severe acquisition footprint (Figure 17). Application of a Footprint Suppression Workflow described by Falconer and Marfurt (2008) met with little success. Even with parameters harsh enough to remove geology the footprint remained apparent (Figure18), therefore; the footprint suppression was abandoned. The footprint runs primarily parallel to the inline direction. Investigation of the footprint along a single crossline (Figure 19) revealed a wave like structure. This wavy structure creates the negative and positive curvature responses and upon closer examination of CRP gathers at those locations a very discrete difference in the amount of residual moveout present can be observed. This difference indicates that the footprint maybe best suppressed through a residual velocity analysis and

also illustrates the high value of attributes being used as a QC for seismic processing.

Attribute analysis was performed on the whitened stacked prestack time migrated volume. Amongst the attributes generated where Sobel filtered similarity, coherent energy, most positive and most negative curvatures, amplitude envelope, instantaneous phase, spectral magnitudes from 10-80 Hz in 2 Hz increments and energy ratio similarity. The seismic amplitude and attribute volumes were then exported in SEG-Y format and imported into a commercial software interpretation package.

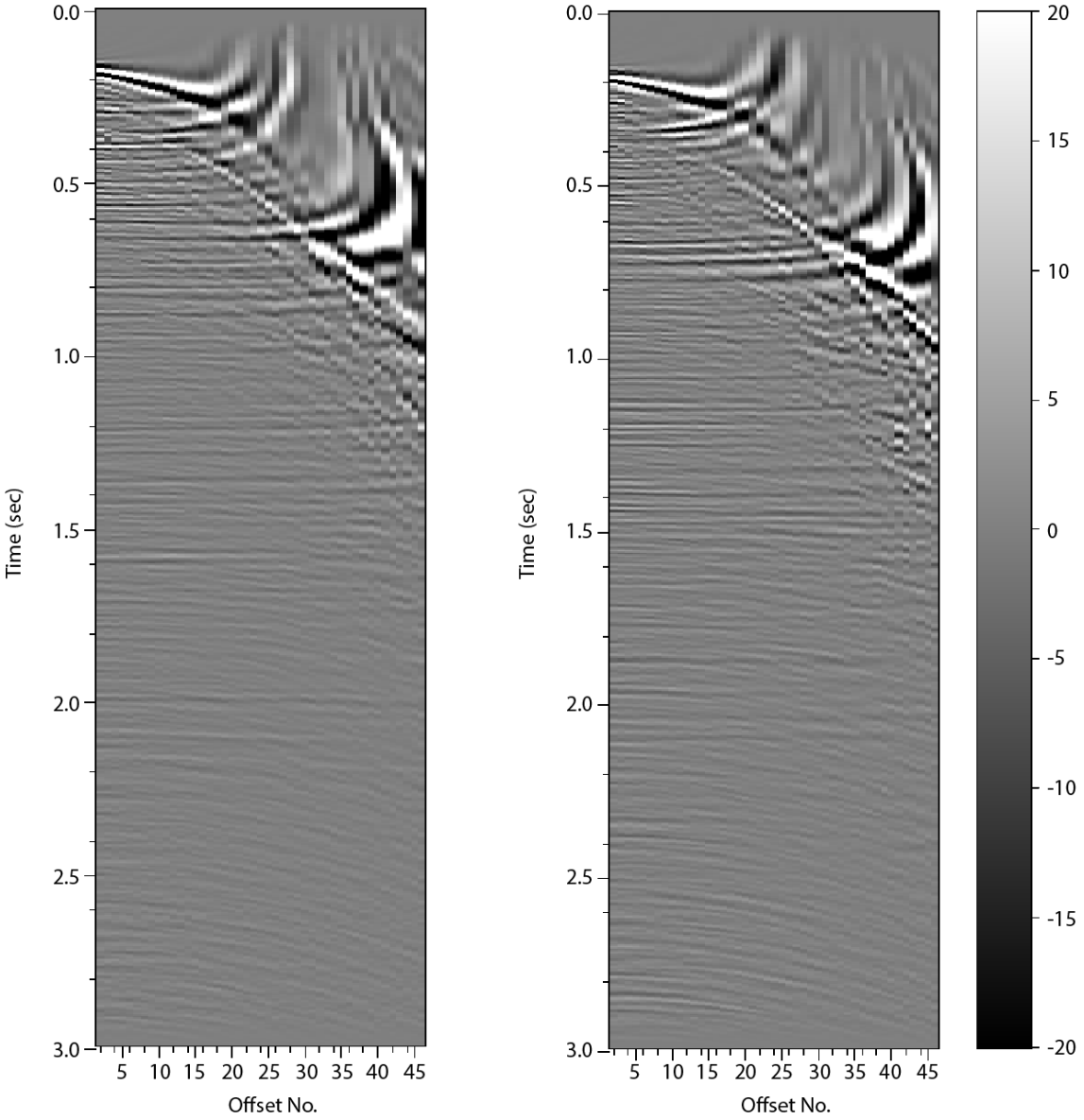


**Figure 14.** CRP gathers after prestack time migration. A small amount of residual moveout can be seen in the far offsets.

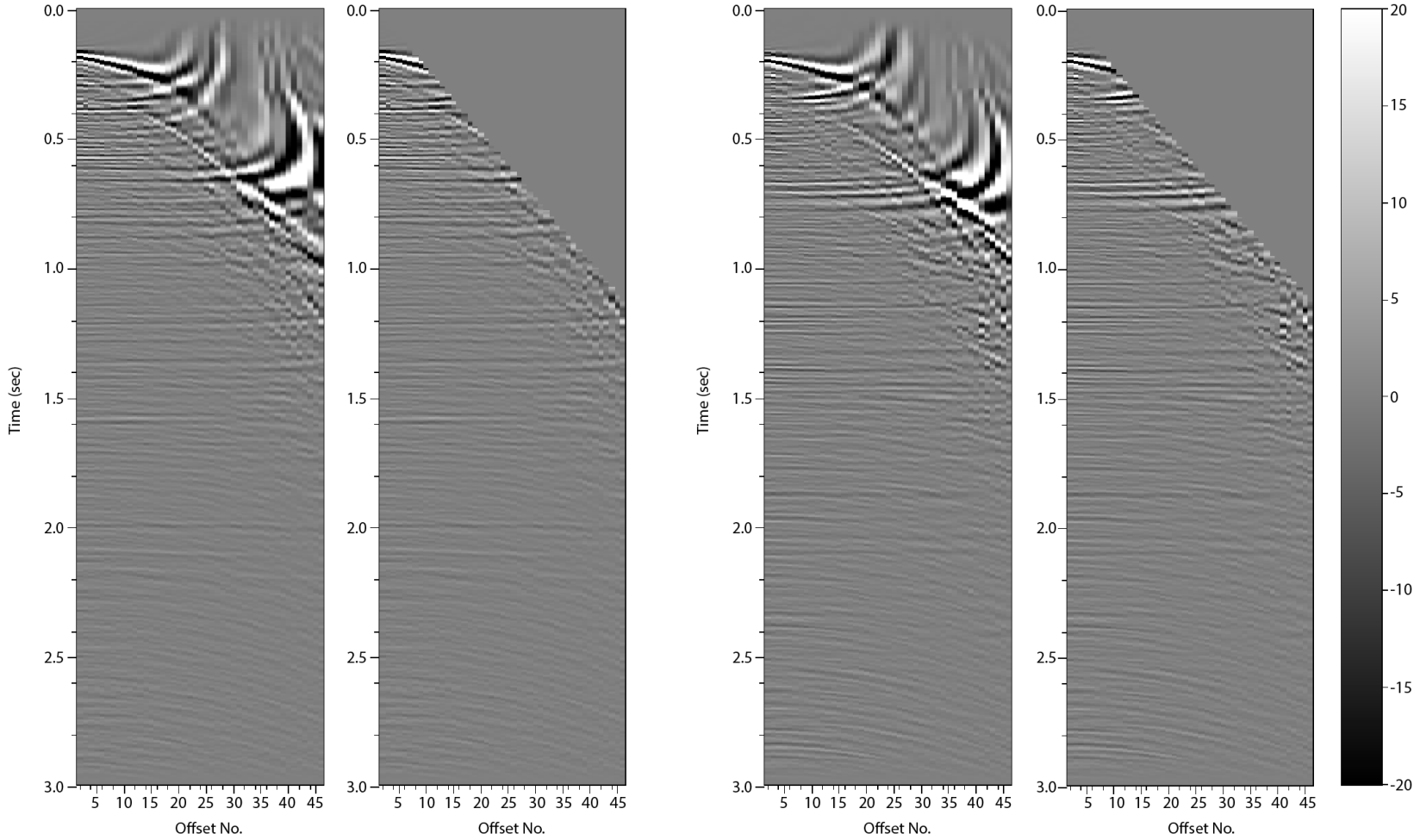


**Figure 15.** Migrated gathers before and after muting to account for NMO stretch. The linear mute is effective in muting the stretch without muting too much of the data.

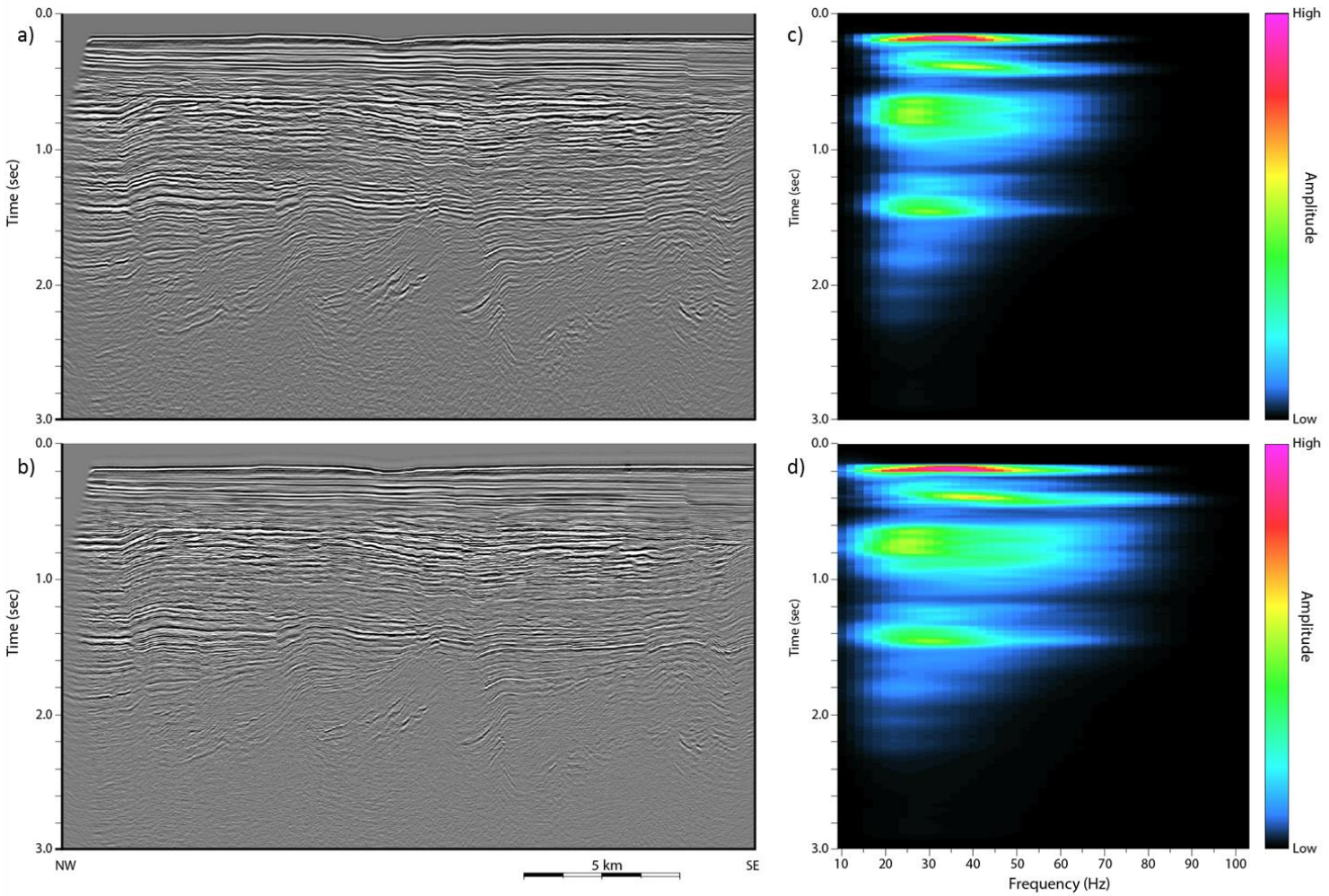


**Figure 16.** Results of the spectral flattening performed in AASPI. (a) Seismic cross-section before flattening and (b) seismic cross-section after flattening demonstrate spectral balancing down to basement focusing the reflectors throughout the section. (c) and (d) show the amplitude spectrum as a function of time with (d) showing a large improvement on the content of the frequency spectra.

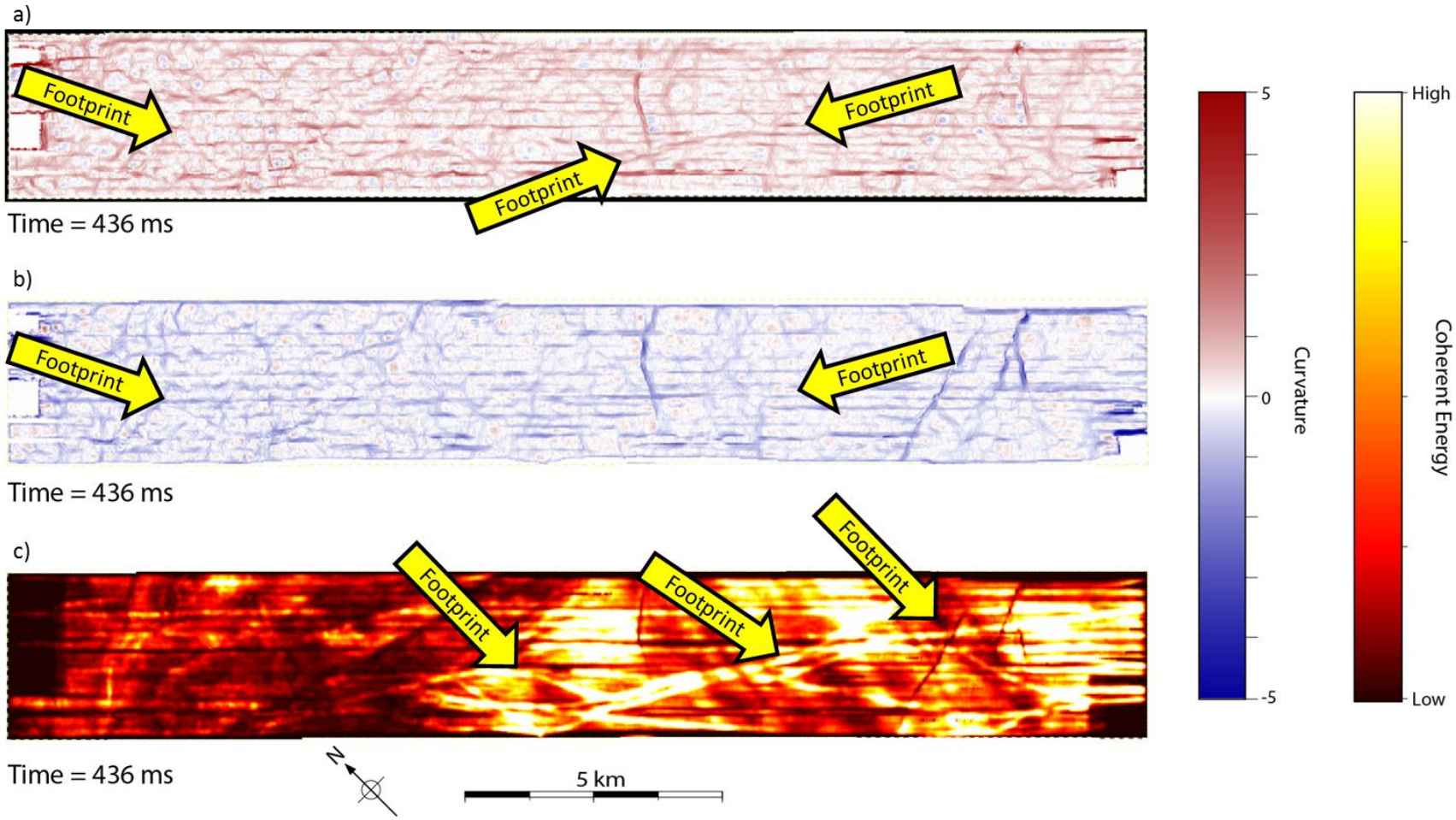


**Figure 17.** Time slices at t = 436 ms across (a) most positive principle curvature, (b) most negative principle curvature and (c) coherent energy showing the effect of the acquisition footprint (yellow arrows) on the attributes.

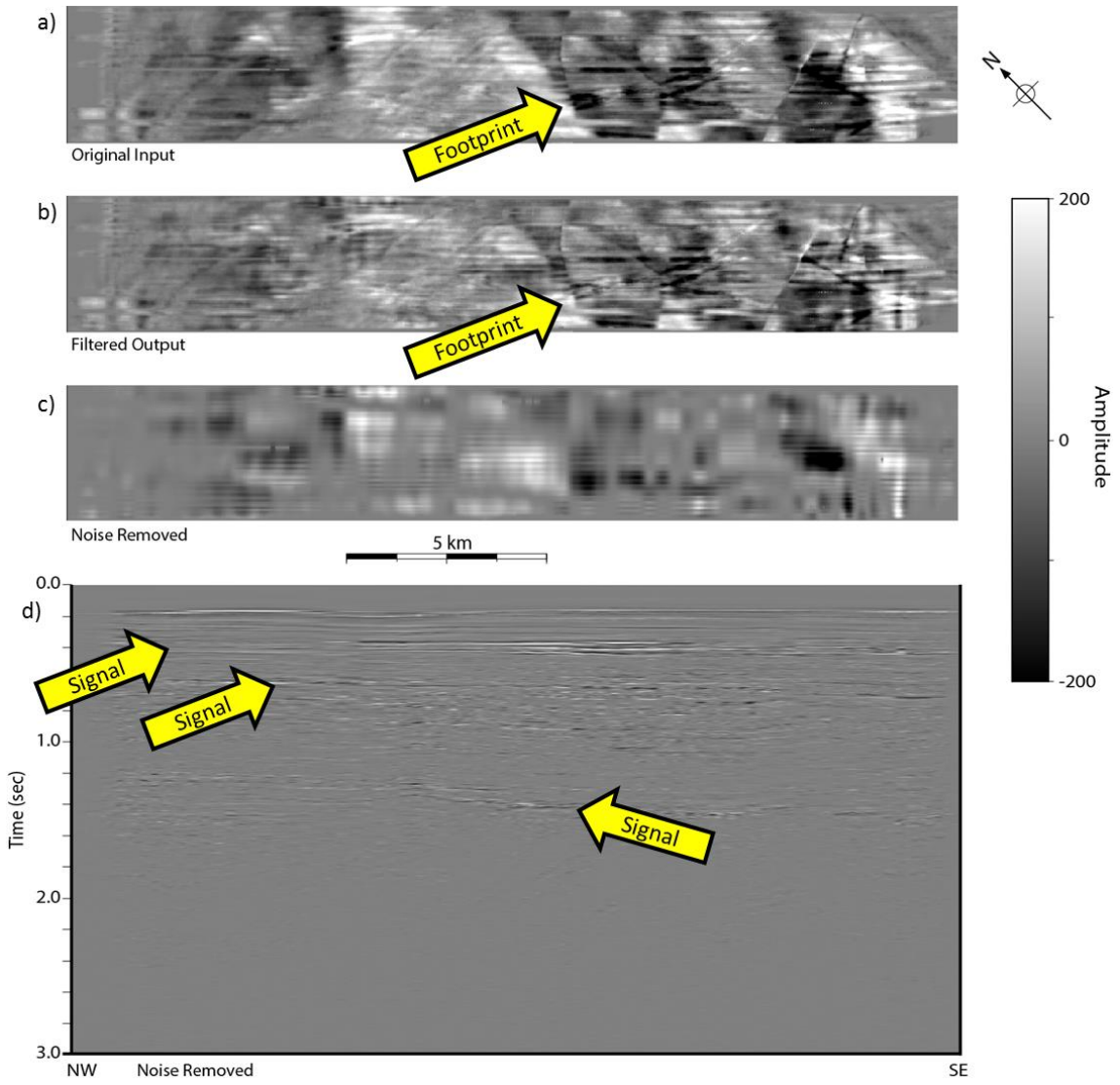


**Figure 18.** Time slices at t = 400 ms showing the (a) original input, (b) footprint filtered data, and (c) the noise removed by the footprint suppression. (d) shows a cross-section of the noise removed by the footprint suppression which resembles more geology than noise.

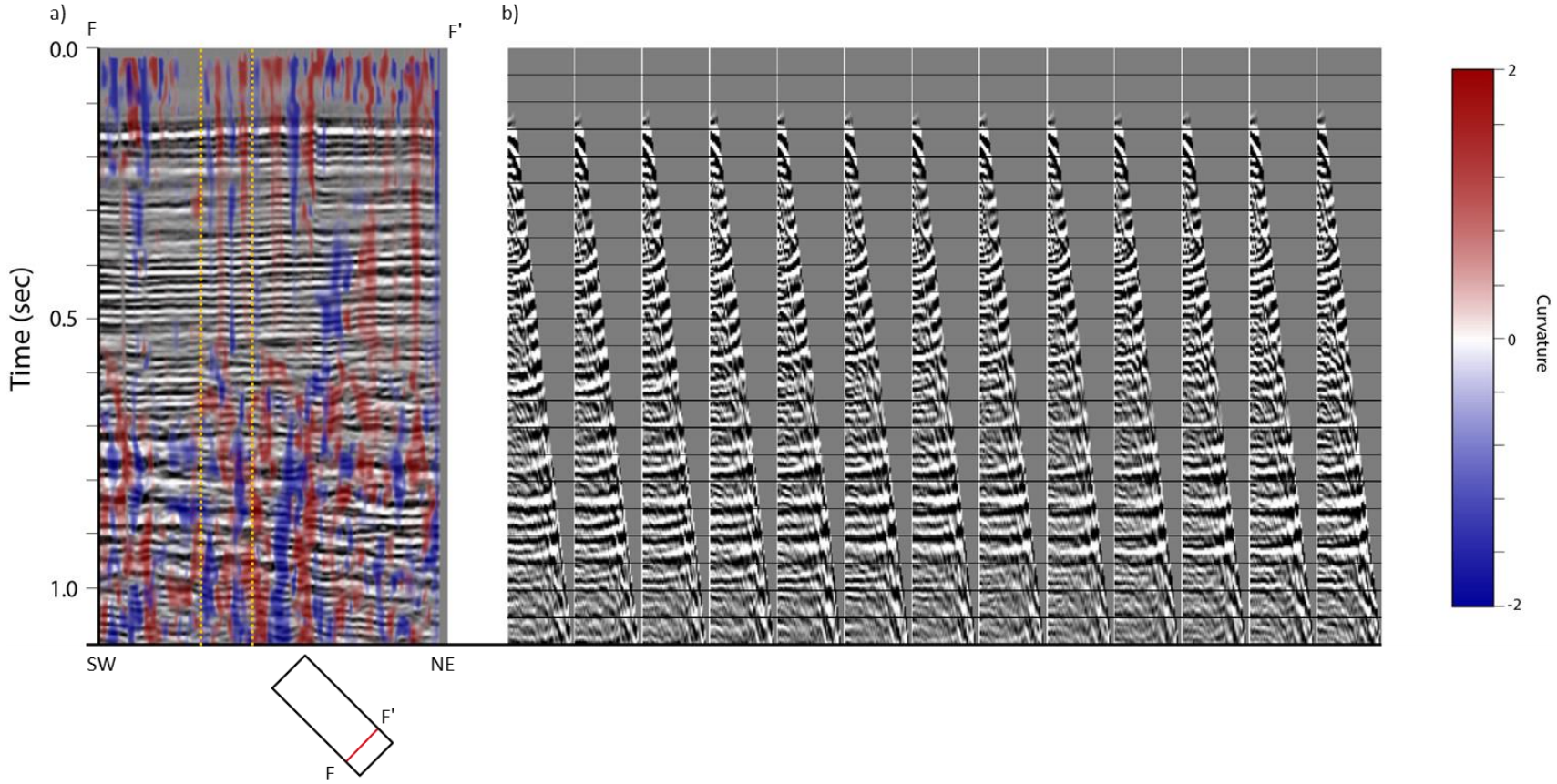


**Figure 19.** (a) crossline view of seismic amplitude with most positive and most negative curvature overlain. The strong curvature anomalies seen in the shallow section correspond to the strong inline curvature artifacts seen in Figure 17. (b) CRP gathers corresponding to traces between the yellow dotted lines in (a) through an anomaly, revealing that in areas of most negative curvature the reflections are flatter, whereas in the areas of positive curvature there is more residual moveout, giving rise to false structural ridges.

## INTERPRETATION

The velocity model indicates low velocities, 1500-3500 m/s, within the sedimentary section. High velocities represent basement rocks past 3 sec. The resulting stacked prestack time migrated data volume rendered a good image of the subsurface, with some clear continuous reflectors, sharp offsets of reflectors in time and a clear acoustic boundary before 3 secs (end of data processed). The data are densely sampled along the inline direction and coarsely sampled in the crossline direction with a nominal bin size of 25 x 6.25 m. Unfortunately, due to weather conditions during acquisition the data suffer from severe acquisition footprint (Figure 17). Irregularities in acquisition also give rise to lateral dimming and brightening of some reflectors (Figure 20). Such irregularities could be remedied by 5D interpolation, some other form of regularization, or least-squares migration (Guo, S., 2012). Conventional Kirchhoff migration does not account for irregular sampling. Least-squares migration, however, computes a reflectivity image that least fits the surface data, such that a denser data provides more constraints rather than a stronger amplitude (Guo, 2012).

The whitened data volume showed significant increase in resolution compared to the pre-whitened data volume (Figure 16). White block arrows indicate shallow reflectors while yellow block arrows indicated deeper reflectors that have been focused. The attribute volumes generated on the whitened volume prove quite detailed as well. The Sobel filtered similarity illuminates data edges very effectively (Figure 18), along with the most negative curvature. The most positive curvature was highly influenced by the acquisition footprint

diminishing its effectiveness. The coherent energy and energy ratio similarity, while highly sensitive to the acquisition footprint, proved useful in delineating more subtle amplitude features.

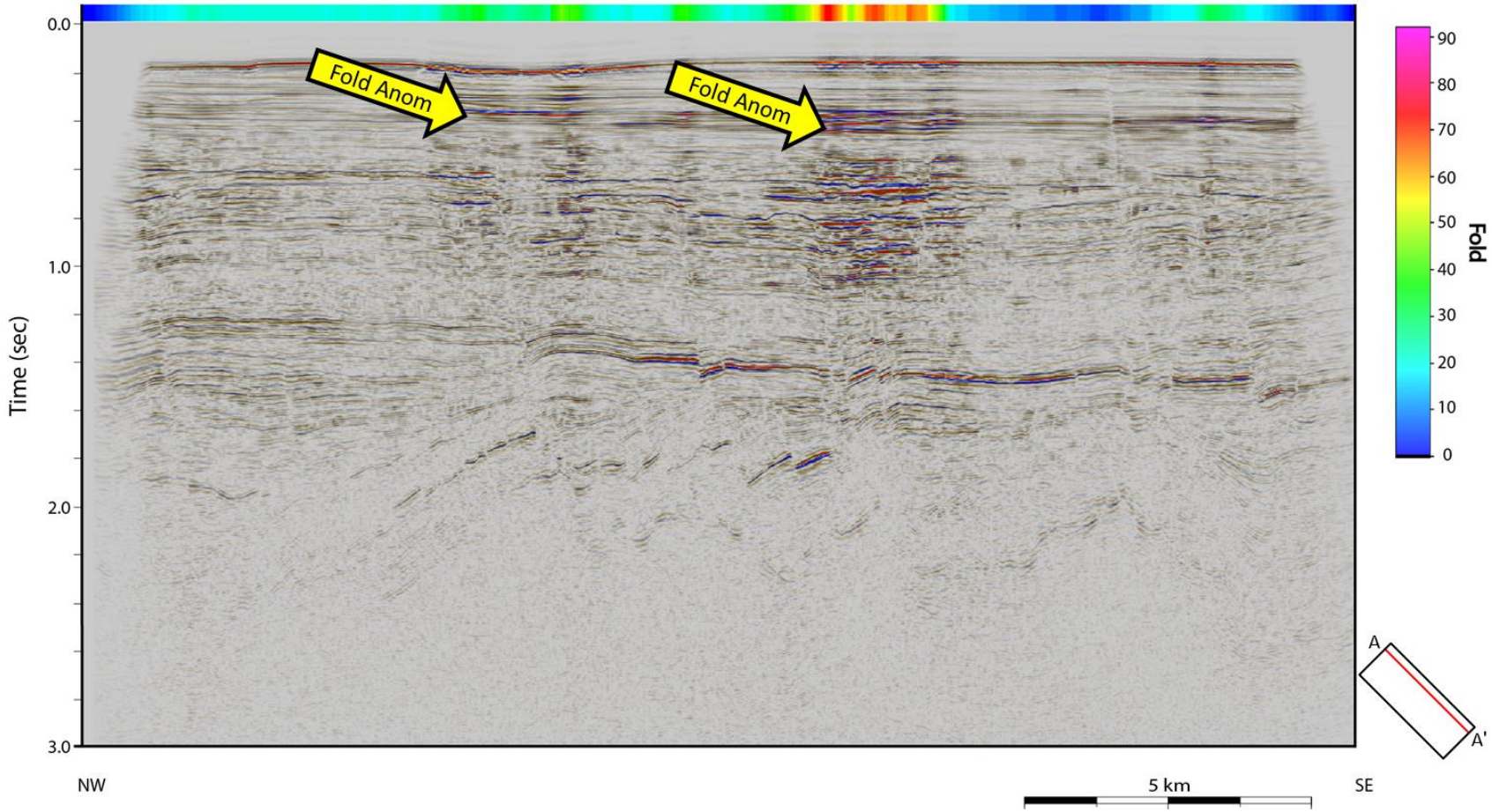


**Figure 20.** Seismic amplitude cross-section illustrating the variation of amplitude with fold (yellow arrows). A fold line has mapped to the upper portion of the slice and a clear correlation exists between the fold and amplitude of each trace.

## STRUCTURAL INTERPRETATION

Figure 21 illustrates many of the key structural features in the area. The area is highly faulted especially in the lower section closer to the basement. Several of the faults (in blue) extend from the basement up almost to the surface indicating recent reactivation along these faults. All of the faults are normal faults along with many conjugate fault systems (in red), consistent with the extensional setting that formed the basin. Literature indicates the presence of an inversion period that most likely reactivated many of these normal faults as reverse faults but there is little if any sense of reverse motion on the faults seen in this data volume. The lack of reverse motion indicates that any reverse motion experienced did not reach the null point for a majority of the length of the fault.

Although many of the faults are vertically extensive and can be easily picked in cross-section even down to basement, they are quite discontinuous in lateral extent (Figure 22). Time slices through good structural attributes are critical to fault correlation.

Most of the small scale folding in this region is likely due to the extension giving rise to rollover anticlines adjacent to the normal faults. Another possibility is the inversion period known as the Longjing Movement, but with no thrust faults present within the surveyed area it is hard to determine if enough shortening occurred to cause folding. A hypothesis to support this can be created if the small scale folds are in fact reverse drag folds. While reverse drag folding typically forms synclines in the footwall, the structural deformation is much less than that of the anticline formed in the hanging wall (Schlische, 1995) and will thus be

harder to image. In reality the small scale folds may have been initially rollover anticlines and then accentuated by compression as reverse drag folding. Either way, the folds adjacent to faults create a strong negative curvature that allows for better fault imaging (Figure 23). The high negative curvature response is due to the sharp drop along the fault in combination of the anticline adjacent to that drop creating a large valley like structure (Figure 24).

The large scale folding across the region illustrates one low amplitude anticline-syncline structure. Unfortunately due to the large scale, low amplitude and intense acquisition footprint this feature is not apparent in any of the structural attributes such as curvature. This structure is truncated by an erosional surface creating a prominent angular unconformity. This erosional surface indicates that the folding caused enough uplift to expose the rock surface. The unconformity is also cut by a few larger faults in the region, almost to the surface, indicating that the tectonics within the basin were recently still active. These large faults are normal in motion signifying that there is still some degree of extension in the Jeju Basin.

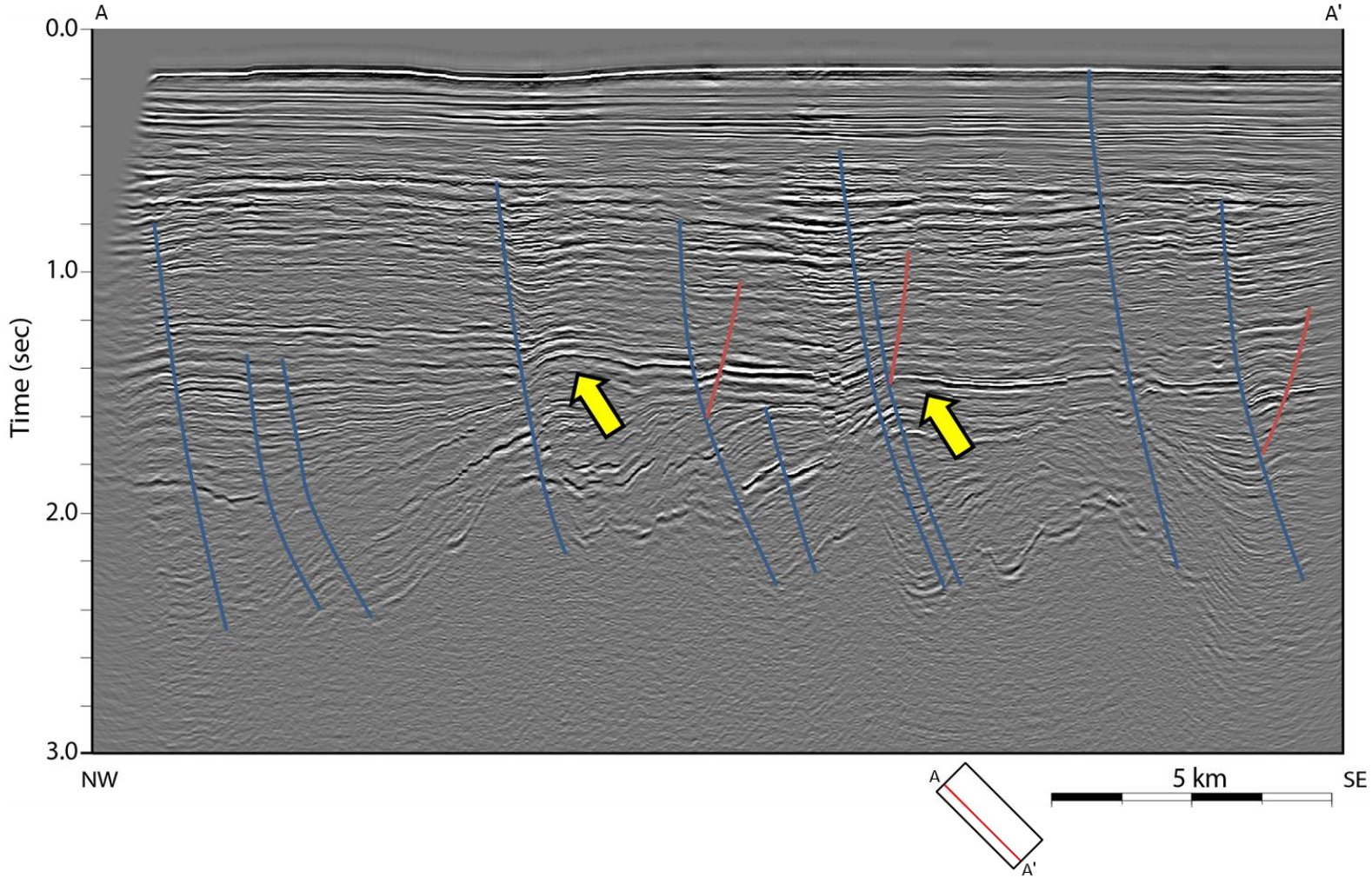


**Figure 21.** Structural interpretation along a representative seismic line showing normal faults (blue), conjugate faults (red), rollover anticlines (yellow arrows) and the low amplitude large scale regional anticline.

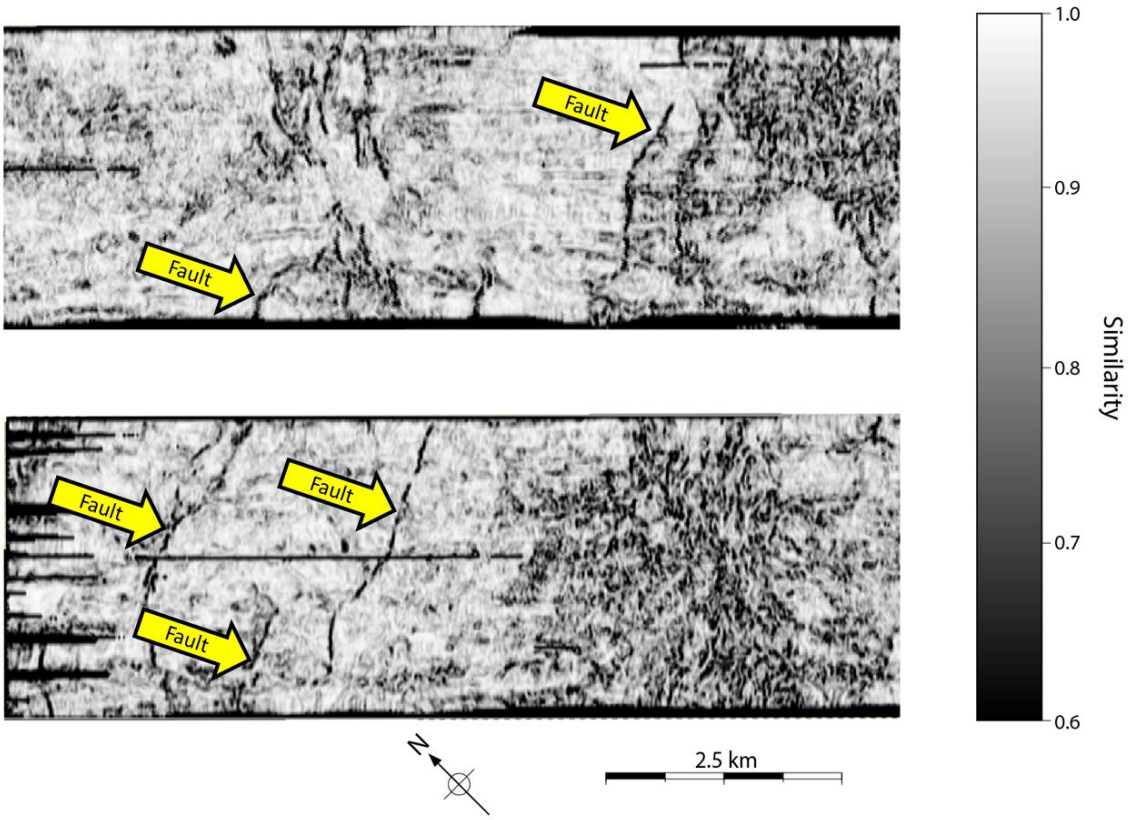


**Figure 22.** Sobel filter similarity time slices at (a) 1300 and (b) 1450 ms illustrating the faults (yellow arrows) and their lateral discontinuity present in the Jeju Basin.

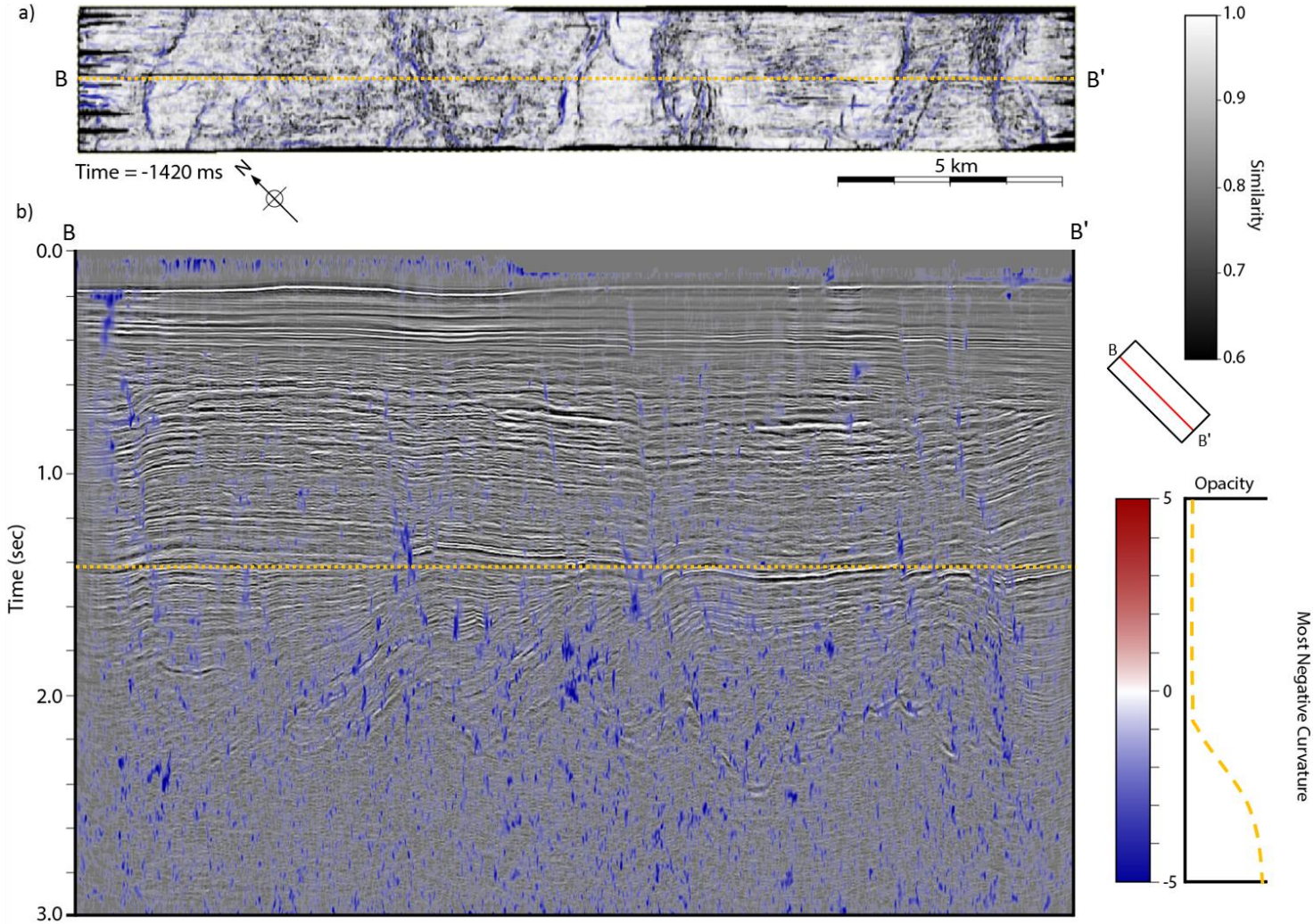


**Figure 23.** (a) Sobel filter similarity overlain with most negative principle curvature at time 1420 ms and (b) a cross-section of seismic amplitude overlain by most negative principle curvature illustrating the strong correlation between negative curvature and faulting within the Jeju Basin.

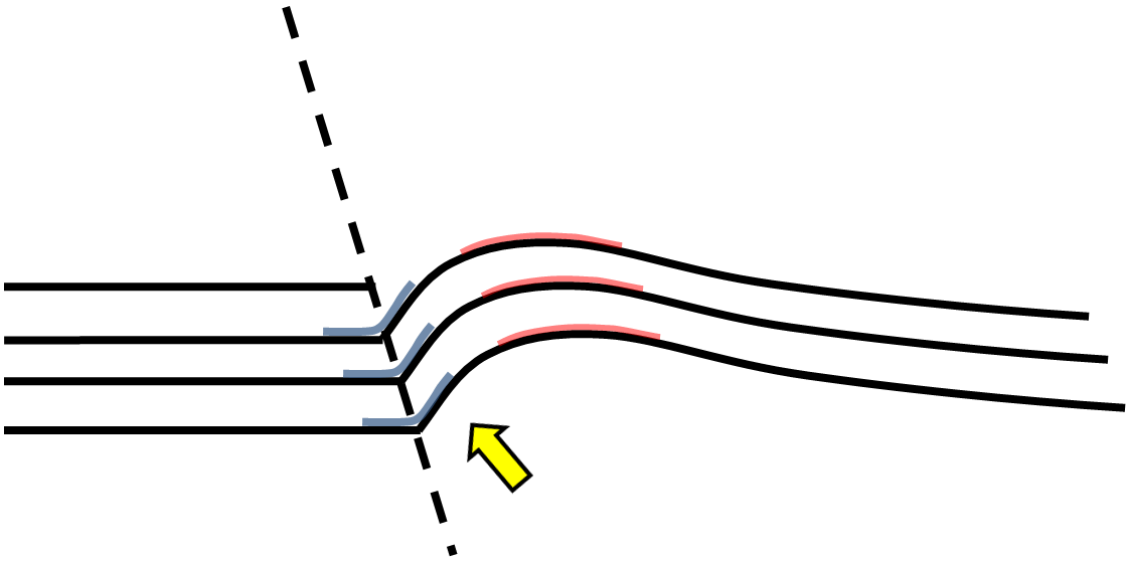

**Figure 24.** Cartoon illustrating the high correlation between the faults and the (blue) most negative curvature due to the (yellow arrow) valley like structure created by a fault adjacent to a rollover or reverse drag fold.

## STRATIGRAPHIC INTERPRETATION

Figure 25 denotes the interpreted megasequence boundaries (MB) discussed earlier. The MB's were interpreted based on comparison to other 2D seismic in the Jeju Basin that has been tied to well data (Cukur et al., 2001). Although not all MB are present in the survey area those MB that are present will be denoted as they are in previous work for consistency. Megasequence 1 and Megasequence 2 are very hard to distinguish and in some shallower areas of the Jeju Basin a boundary is not present. This study area appears to be one such area. Within these first two megasequences (MS1-2) there is a very high degree of faulting, tilting the beds to very high angles. The horst and graben structures are easily identified along with the acoustic basement. Syntectonic deposition along growth faults give rise to thicker sequences closer to the fault on the hanging wall side. Such patterns are easily seen on seismic amplitude and instantaneous phase (Figure 26).

Megaboundary 3 separates MS1-2 from MS3 is readily identifiable (Figure 25). The boundary was picked based on the lack of growth along the faults indicating that significant extension had ended. The reflectors within MS3 change significantly throughout the section dividing MS3 into two distinct sections. In the lower portions of MS3 the reflectors appear very smooth with good separation. There also appears to be a very bright extensive bed that maintains high amplitude across faults despite the displacement. The high amplitude bed becomes very apparent when looking at any attribute based on energy (i.e. Amplitude Envelope and Coherent Energy) as seen in Figure 27 (of the coherent

energy). The high positive amplitude indicates a high impedance contrast with lower body being faster and denser. The high positive amplitude along with the continuity of amplitude strength across faults indicates that this is most likely an igneous body. Sills and other igneous bodies are a common occurrence in the Jeju Basin and the timing of this event early in the deposition of MS3 corresponds with the timing of other igneous events found in the area (Cukur et al., 2010). The body has experienced the same amount of displacement along faults as surrounding units indicating that the faulting occurred after emplacement and is interpreted to likely be a lava flow that occurred on the surface as opposed to a sill that should appear more continuous experiencing less displacement.

The upper section of MS3 is much more chaotic with many reflectors close together that are not very continuous and frequently form a channel like shape or truncation. The upper section also displays some channel features that are seen on timeslices (Figure 28, 29, and 30). These channel features are difficult to identify in timeslice with the seismic volume alone but with the attributes identification becomes much less difficult. The attributes Sobel filter similarity, coherent energy, energy ratio similarity, along with spectral magnitudes at the higher frequencies were particularly useful in the recognition of channel features. While not easily seen in time slice along the fold of the entire MS3 sequence the channels can be seen in the flatter portions of the upper section. Flattening along a carefully picked horizon and extraction of attributes along that surface may yield a more continuous image of the channel systems present.

MS3 is truncated by an erosional boundary that forms an angular unconformity that establishes MB4 and is overlain by MS4. The angular unconformity is non planar and displays a small amount of displacement along the few faults that extend through it. The overlying MS4 unit, as reported by Lee et al. (2006) and Cukur et al. (2011), divides itself into two subunits. The two sections can be easily identified looking at the instantaneous frequency attribute (Figure 31) along with any of the similarity attributes (Figure 32). The lower section is characterized by less continuous more chaotic reflectors, interpreted to be a more terrestrial marine coast environment, while the upper section has much clearer continuous reflectors indicating a more marine setting. Only a few of the larger faults in the region penetrate the MS4 and appear to extend almost to the surface.

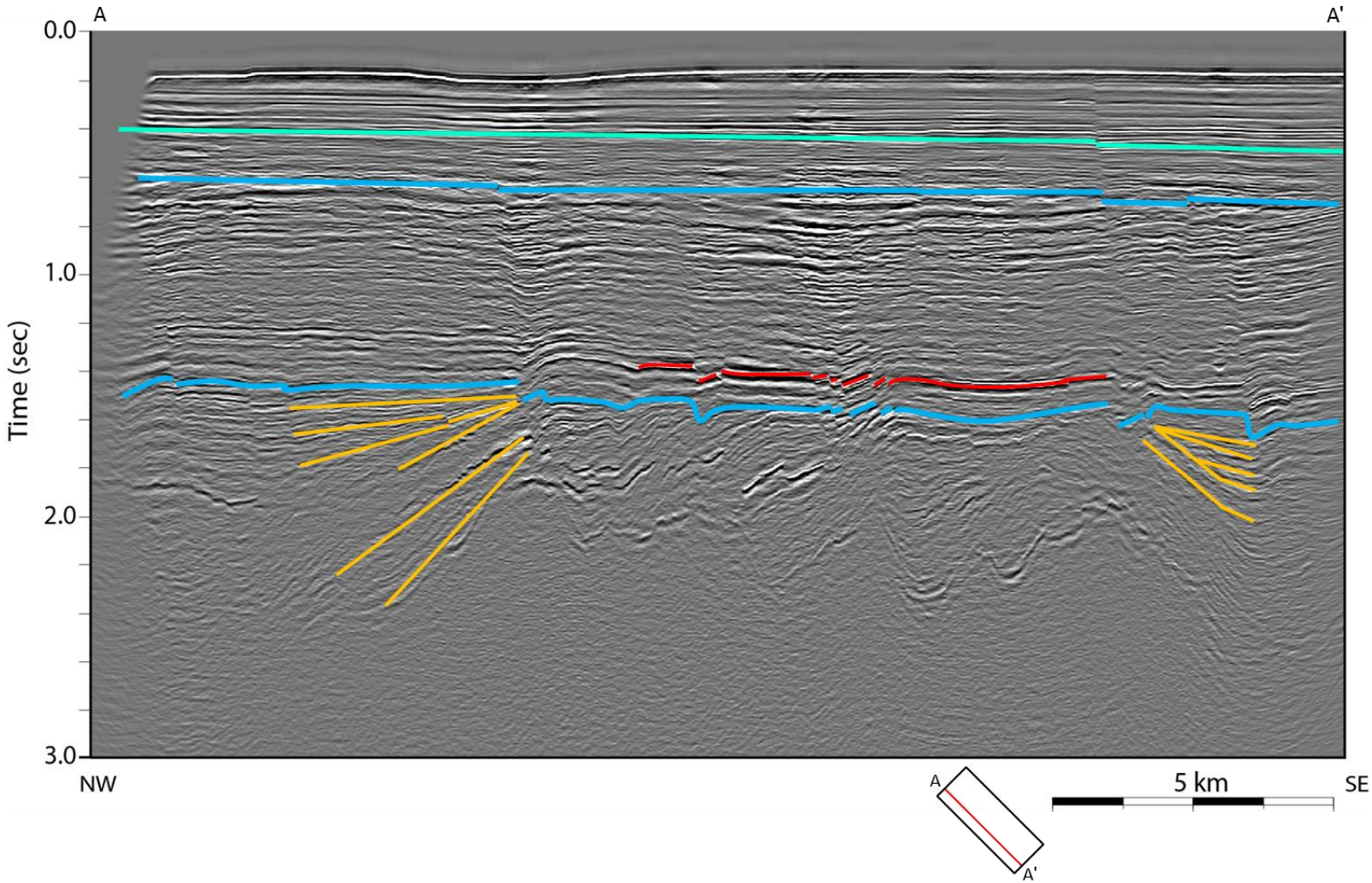


**Figure 25.** Stratigraphic interpretation along a representative seismic line highlighting the megasequences and their boundaries (blue), including the marine boundary in MS4 (teal), along with the growth fault deposition (orange), in the MS1-2 and the interpreted igneous body (red).

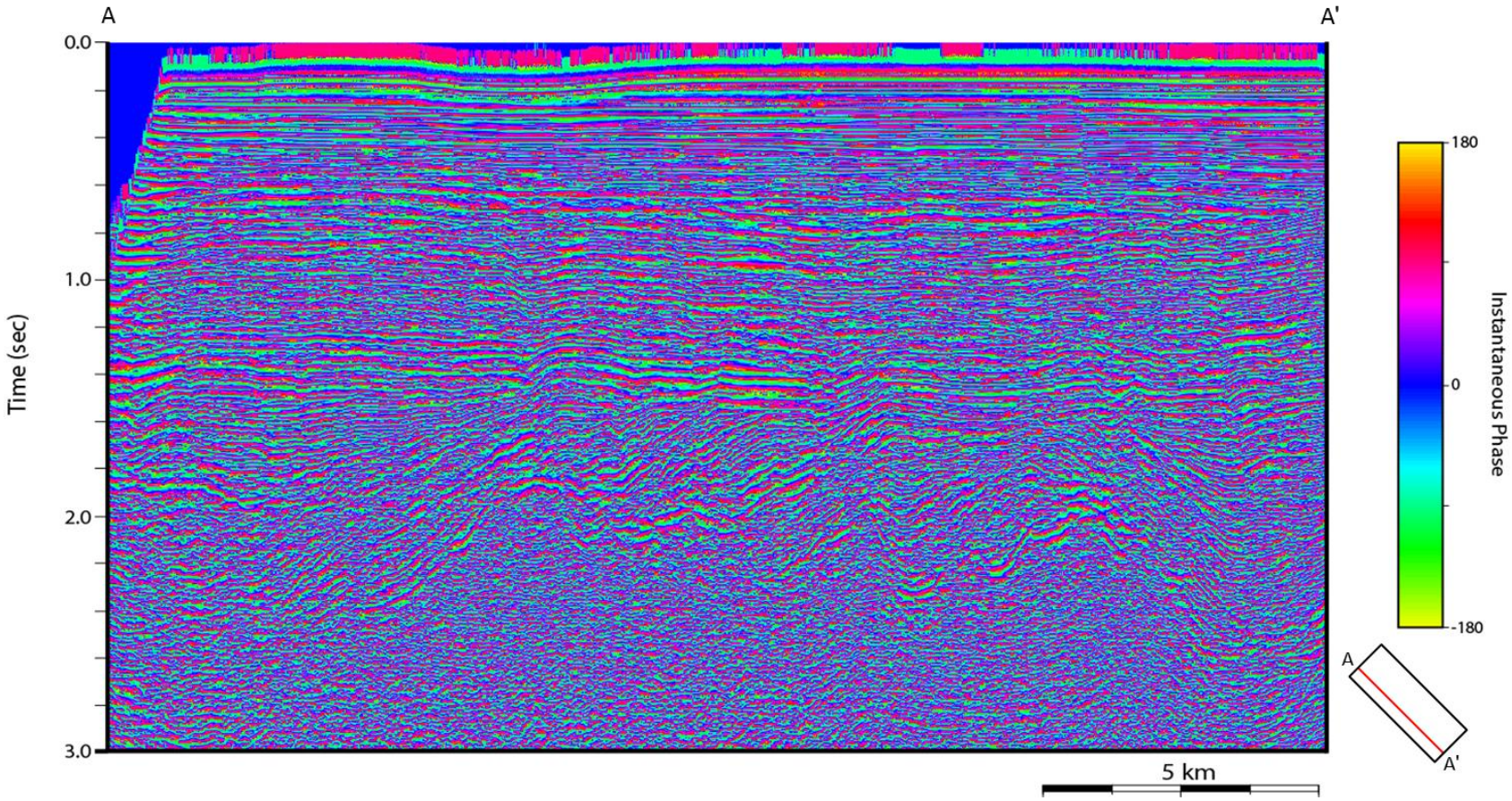


**Figure 26.** Cross-section of instantaneous phase emphasizing the fan shape of the growth fault deposition and the acoustic basement.

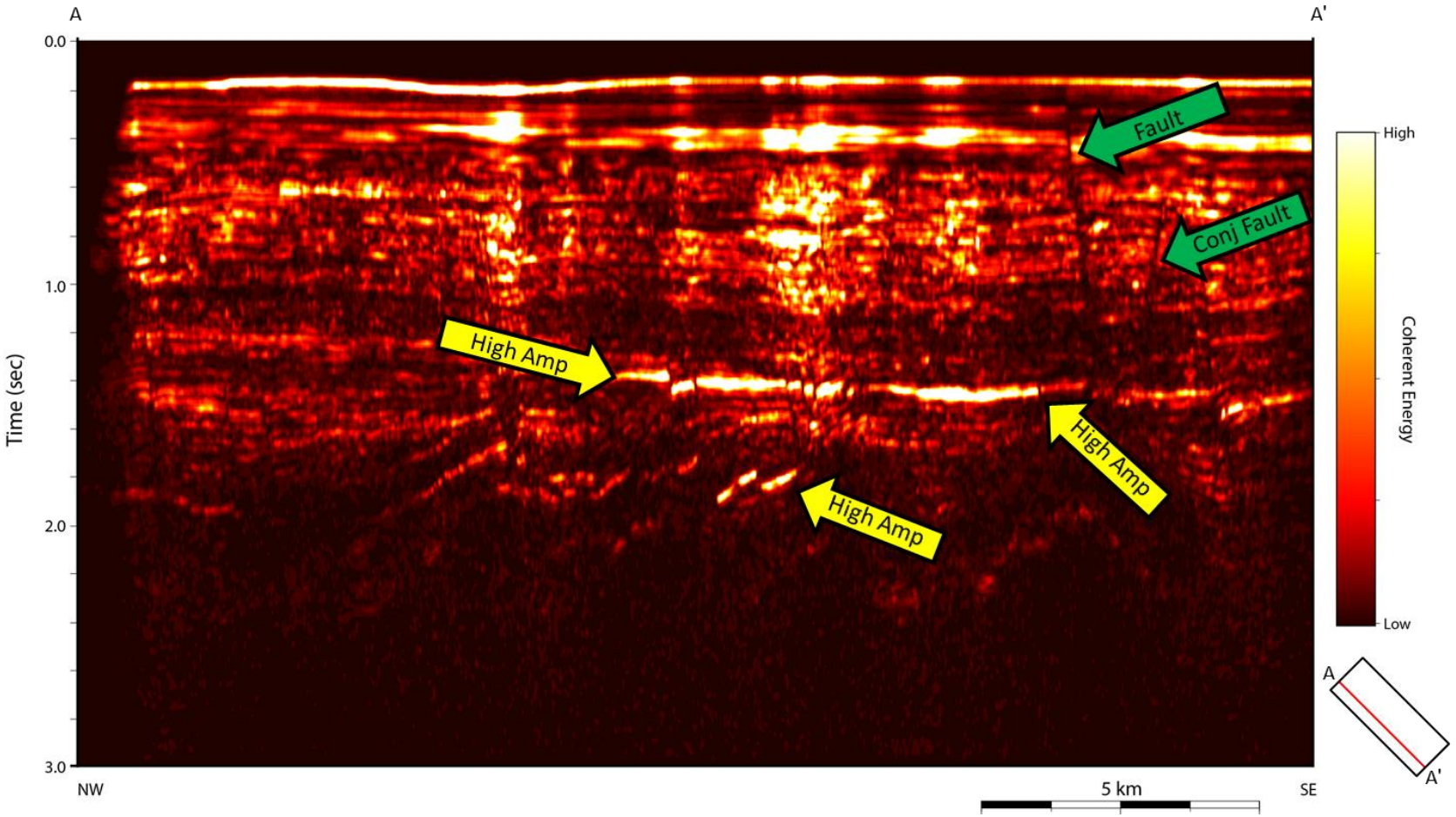


**Figure 27.** Coherent energy cross-section highlighting some of the high amplitude anomalies (yellow arrow) and faults (green arrows). The lower amplitude anomalies are interpreted to be geological whereas the higher anomalies, < 1.0 sec, are most likely due to irregular sampling as seen in Figure 20.

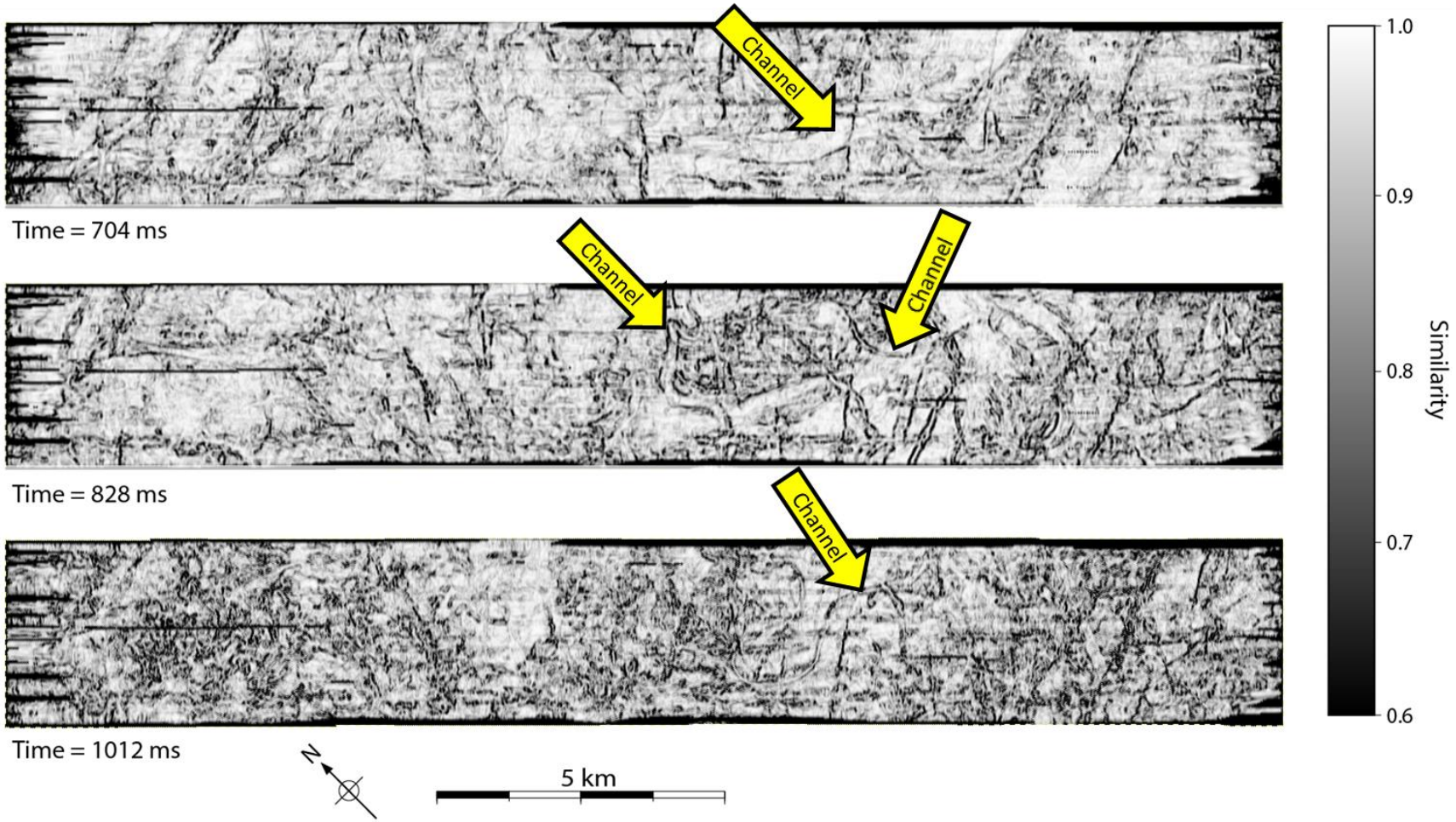


**Figure 28.** Sobel filtered similarity illustrating some of the more prominent channel systems (yellow arrows) within the basin.

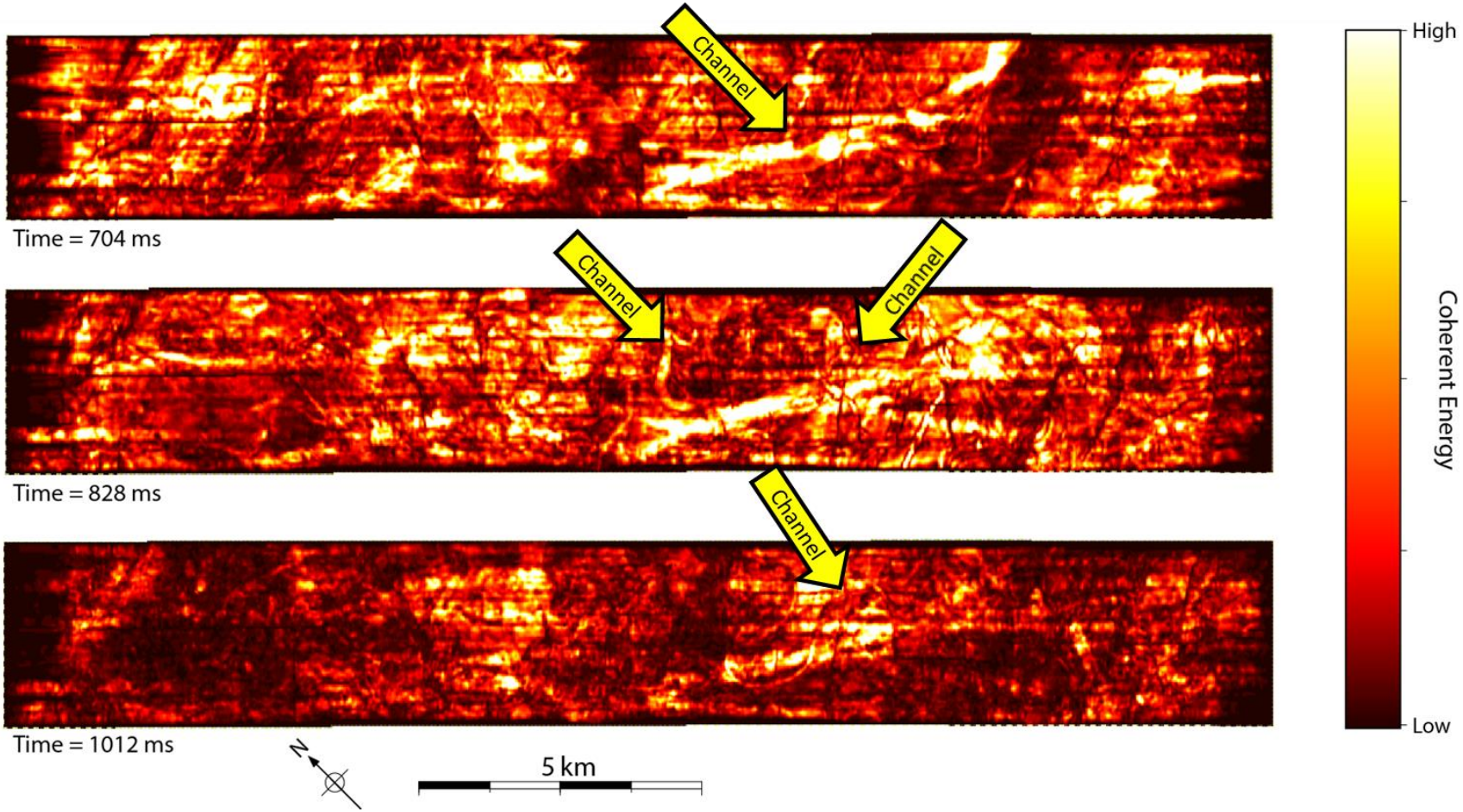


**Figure 29.** Coherent Energy Time slices illustrating some of the more prominent channel systems (yellow arrows) within the basin. A bright footprint anomaly can be seen in all images crossing diagonally across the survey.

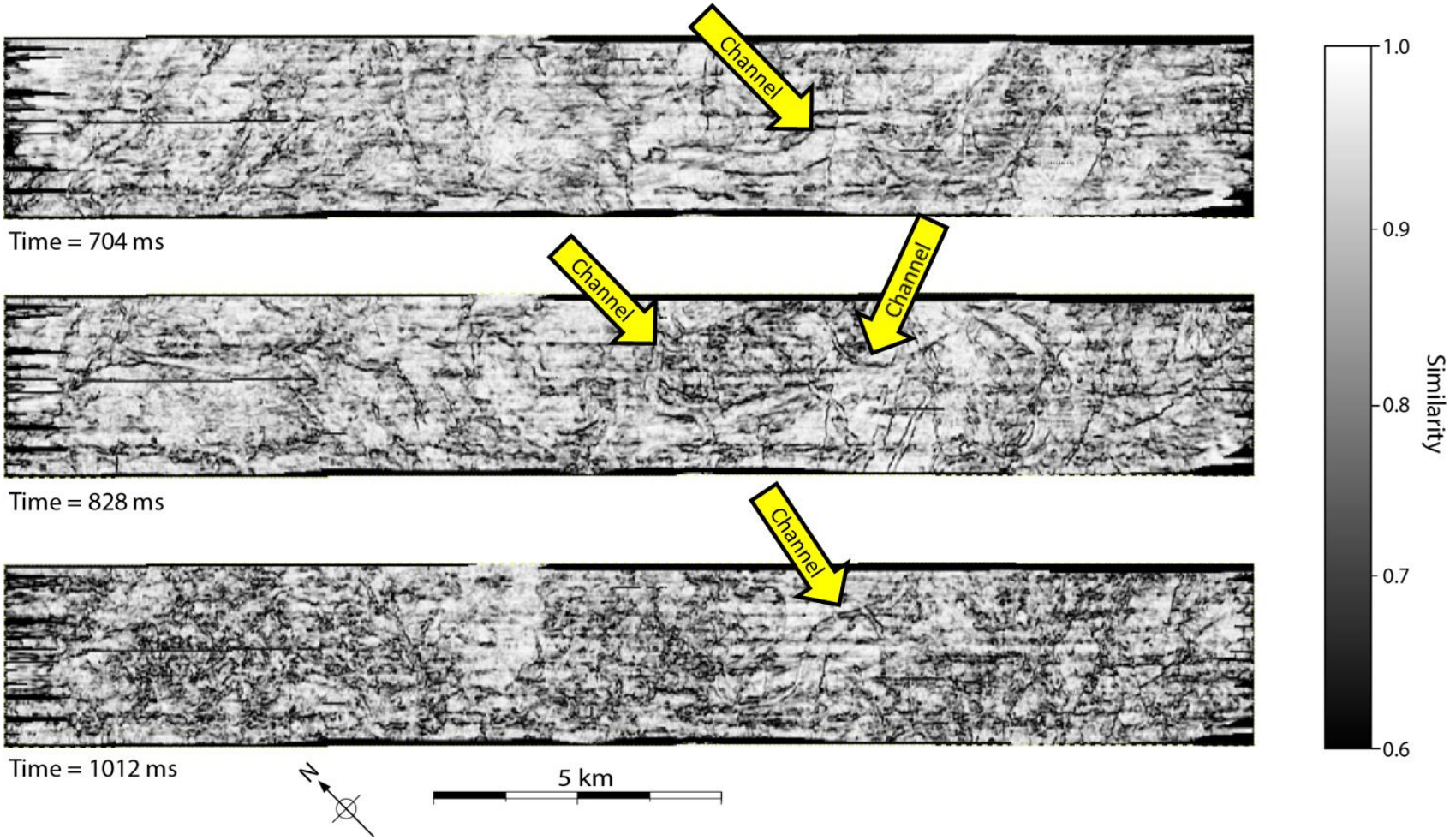


**Figure 30.** Energy ratio similarity being more sensitive to small scale changes than Sobel filtered similarity better illustrates some of the channel systems (yellow arrows) present within the basin.

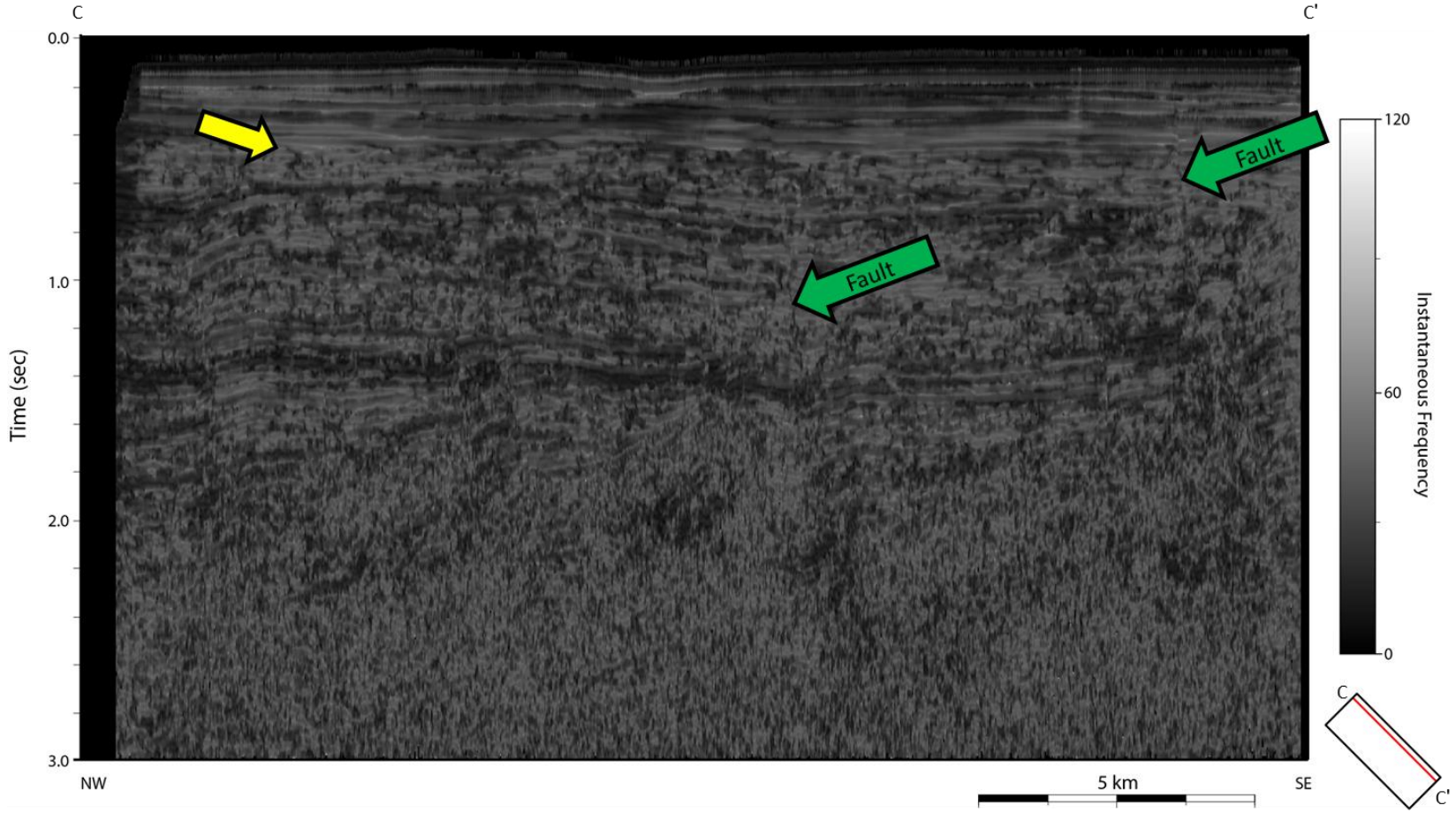


**Figure 31.** Instantaneous frequency cross-section highlighting the marine boundary (yellow arrow) in MS4 along with some faults (green arrows).

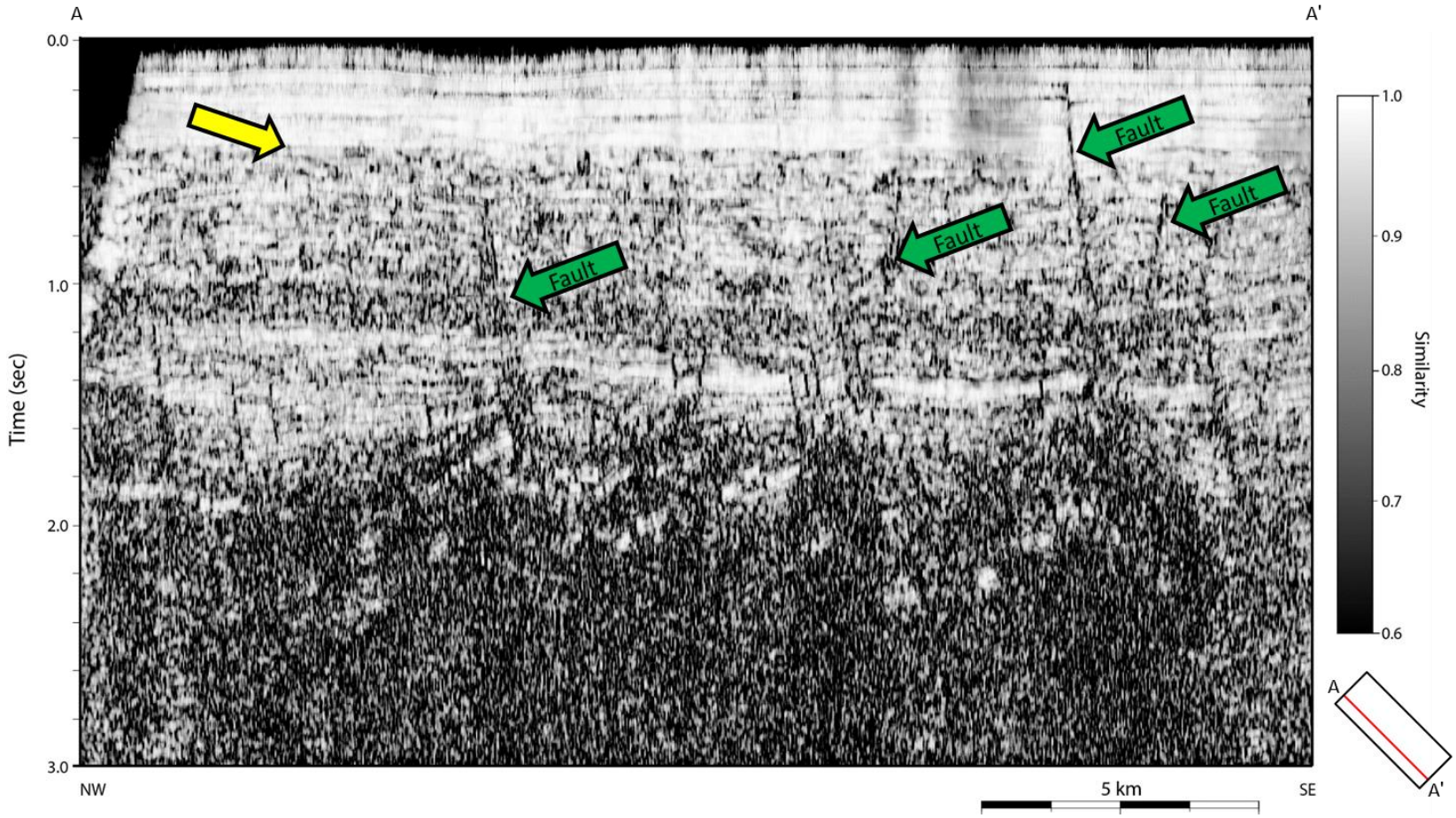


**Figure 32.** Cross-section of Sobel filter similarity imaging the faults very well (green arrows) as well as highlighting the break (yellow arrow) between what is interpreted to be the marine and non-marine portions of MS4.

## AMPLITUDE ANOMALIES AND POTENTIAL HYDROCARBON TRAPS

One of the primary purposes of this study was to identify potential hydrocarbon resources within the Jeju Basin. While this study only represents phase 1 of a multiyear acquisition program, several preliminary observations about seismic acquisition and hydrocarbon systems in the area can be made. A major observation has to do with amplitude preservation. While 3D seismic data can be successfully acquired with only two streamers and two gun arrays resulting in 4 lines of CDP gathers for each pass of the boat, consistent subsurface illumination requires very precise driving of the boat and minimal currents in order to minimize streamer feathering. Such narrow azimuth collection gives rise to strong the acquisition footprint. To alleviate these problems one needs to either weight the value of each trace or interpolate the irregularly sampled data into a regular grid.

Without such correction, any sort of direct hydrocarbon indicator (DHI) should be evaluated for amplitude anomalies created by a sharp increase or decrease in fold. These fold effects are most apparent in the shallow section (Figure 20) and skew attributes that prefer consistent fold (Figure18). Amplitude anomalies are also associated with igneous bodies in the Jeju Basin. Identification of the full petroleum system (source, trap, seal, migration, and timing) is the preferred method for identification of potential hydrocarbons. Later stages of data collection set will include the Dragon 1 well which will be critical in identifying such components.

In addition to the high amplitude body in MS3 interpreted to be a lava flow, there are several other high amplitude bodies in the deeper, heavily faulted MS1-2 (Figure 33). These areas are fairly easily seen on seismic amplitude and are highlighted with the coherent energy attribute. Areas that are deeper would be closer to previously identified source rocks and would have existed with a potential trap prior to the generation of oil allowing for its accumulation, (Cukur et al., 2012) whereas the MS3 group would have lacked a structural trap at the time of oil generation as it predates the folding inversion event. These deeper high amplitude anomalies truncate into faults indicating a possible seal and do not have a consistent amplitude across faults indicating that there is some property of the rock that is different from one side of the fault to the other. The amplitude response from them is also that of a high negative amplitude indicating a negative impedance contrast, which is consistent with a gas charge reservoir.

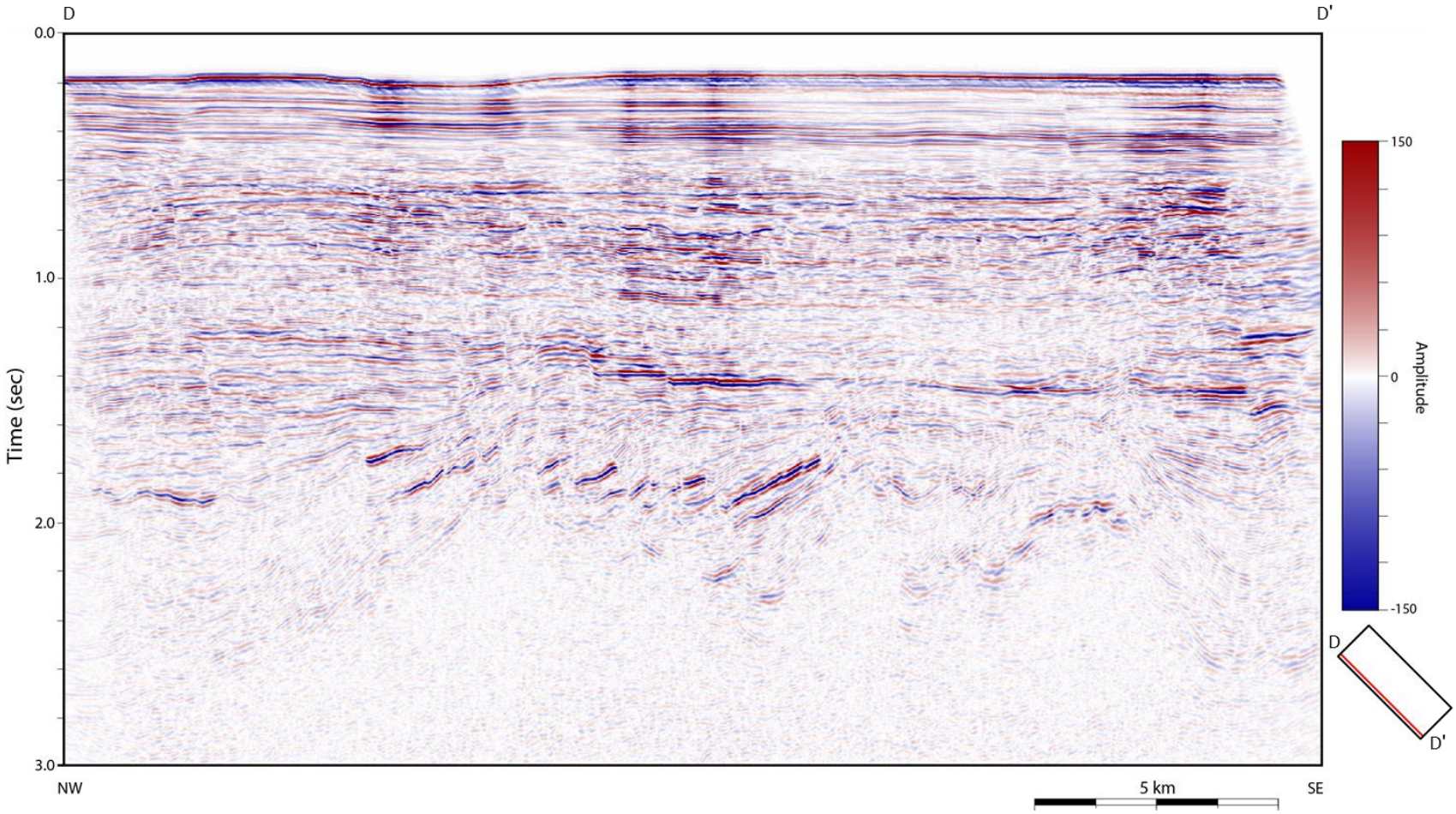


**Figure 33.** Seismic amplitude cross-section demonstrating some of the lower (MS1-2) amplitude anomalies that could hold potential for HC exploration (yellow arrows) and the interpreted igneous body (blue arrow).

# CONCLUSIONS

The 3D marine seismic acquired by KIGAM's phase 1 program are of excellent quality and after careful processing accurately map the geology down to basement. The water bottom gives rise to severe surface related multiples that were eliminated by applying 2D SRME to the 3D dataset, sail line by sail line. Prestack time migration provided subsurface images with little to no migration artifacts. Upon stacking, a very strong acquisition footprint was recognized that severely affects the shallower part of the data. These negative effects can be partially mitigated by additional velocity analysis of the migrated data followed by remigration of the original data.

Seismic attributes are effective in mapping and correlating complex faults. Seismic amplitude and attributes show three of the four megasequences reported by Cukur et al. (2012) to be present in the survey area. Many different sedimentary features exist within the megasequences. MS1-2 have been highly faulted and have been tilted to a high degree of dip. The presence of growth faults can be detected within MS1-2 by the presence of sedimentary packages that thicken towards the faults. As suggested by Cukur er al. (2012) MS1-2 also appear to have the most promise for HCs in this study area. The MS3 sequence has a lesser degree of faulting but still experienced a significant amount of displacement along major faults, resulting in rollover anticlines. Most of the conjugate faults in the study area primarily displace packages within the MS3. In the lower portion of the MS3 I interpret a strong reflector to be a lava flow, the timing of which is consistent with known volcanic periods in the region. The upper

section of MS3 is characterized by many fluvial systems. MS3 is also the unit most affected by the large low amplitude fold consistent with the Longjing movement. This fold allowed for uplift and erosion of MS3 and formed an angular unconformity (MB4) with MS4 that is easily identified. MB4 does display a small amount of displacement along faults that both terminate and pass through the unconformity. This indicates that the terminating faults were active after the uplift and erosion of MS3 but stopped prior to the deposition of MS4, while the faults that extend into MS4 appear to still be active as many extend to near surface. Although MS4 lacks easily identifiable terrestrial sedimentary structures it can readily be divided into a lower non-marine and upper marine depositional sections.

These data represent just Phase 1 of a multiphase survey and therefore present multiple stages of processing. For future work the recently received 2013 survey will be incorporated. The migration for the data here presented and future data will be migrated at 25 x 25 m rather than 25 x 6.25 m bins. In order to help compensate for the irregular fold a least-squares migration will be used. Residual velocity analysis will be performed to better flatten the far offsets. Finally, with new data covering the Dragon-1 well a prestack inversion can be completed.

## REFERENCES


Cukur, D., S. Horozal, D. C. Kim, and H. C. Han, 2011, Seismic stratigraphy and structural analysis of the northern East China Sea Shelf Basin interpreted from multi-channel seismic reflection data and cross-section restoration: Marine and Petroleum Geology, **28**, 1003-1022.

Cukur, D., S. Horozal, G. H. Lee, D. C. Kim, and H. C. Han, 2012, Timing of trap formation and petroleum generation in the northern East China Sea Shelf Basin: Marine and Petroleum Geology, **36**, 154-163.

Cukur, D., S. Horozal, D. Kim, G. Lee, H. Han, and M. Kang,2010, The distribution and characteristics of the igneous complexes in the northern East China Sea Shelf Basin and their implications for hydrocarbon potential: Marine Geophysical Research, **31**, 299-313.

Dowdell, B., 2013, Prestack seismic analysis of Mississippi Lime resource play in the Midcontinent, U.S.A.: M.S. Thesis, The University of Oklahoma.

Dragoset, B., I. Moore, and C. Kostov, 2006, The impact of field-survey characteristics on surface-related multiple attenuation: Geophysical Prospecting, **54**, 781-791.

Dragoset, B., E. Verschuur, I. Moore, and R. Bisley, 2010, A perspective on 3D surface-related multiple elimination: Geophysics, **75**, A245-A261.

Duquet, B., K. J. Marfurt, and J. A. Dellinger, 2000, Kirchhoff modeling, inversion for reflectivity, and subsurface illumination: Geophysics, **65**, 1195-1209.

Falconer, S., and K. J. Marfurt, 2008, Attribute-driven footprint suppression: 2008 SEG Annual Meeting, 2667-2671.

Farooqui, M. Y., H. Hou, G. Li, N. Machin, T. Neville, C. Shirivastva, Y. Wang, F. Yang, X. Yang, C. Yin, and J. Zhao, 2009, Evaluating volcanic reservoirs: Oilfield Review , **21**, no. 1, 36-47.

Guo, S., 2012, Noise suppression using precondition least-squares prestack time migration and imaging of Mississippi Limestone: M.S. Thesis, The University of Oklahoma.

Kwon, Y.-I., and S. Boggs Jr., 2002, Provenance interpretation of Tertiary sandstones from the Cheju Basin (NE East China Sea): a comparison of conventional petrographic and scanning cathodoluminescence techniques: Sedimentary Geology, **152**, 29-43.

Lee, G. H., B. Kim, K. S. Shin, and D. Sunwoo, 2006, Geologic evolution and aspects of the petroleum geology of the northern East China Sea shelf basin: AAPG Bulletin, **90**, 237-260.

Lee, G., B. Lee, B.-Y. Yi, K. Lee, M.-h. Park, H.-J. Kim, and H.-S. Yoo, 2012, Estimation of the CO2 storage capacity of the structural traps in the southern Jeju Basin, offshore southern Korea, northern East China Sea: Geoscience Journal, **16**, no. 3, 313-326.

Pigott, J. D., M.-H. Kang, and H.-C. Han, 2013, First order seismic attributes for clastic seismic facies interpretation: Examples from the East China Sea: Journal of Asian Earth Sciences, **66**, 34-54.

Sarkar, S., 2013, Time to Pick? NO Need to Fear 'Seismophobia': AAPG Explorer, January, 32-33.

Schlische, R. W., 1995, Geometry and origin of fault-related folds in extensional settings: AAPG Bulletin, **79**, no. 11, 1661-1678.

Verschuur, D. J., A. Berkhout, and C. Wapenaar, 1992, Adaptive surface-related multiple elimination: Geophysics, **57**, 1166-1177.

Weglein, A., 1999, Multiple attenuation: an overview of recent advances and the road ahead : The Leading Edge, **18**, 40-44.

Zhang, K., K. J. Marfurt, Z. Wan, and S. Zhan, 2011, Seismic attribute illumination of an igneous reservoir in China: The Leading Edge, **30**, 266-270.

## APPENDIX A: 2D SRME ON 3D MARINE SEISMIC DATA

A significant accomplishment of my thesis was determining how to utilize 2D SRME on a 3D data set. This required a significant amount of patience and outside the box thinking. I write this appendix to give a brief yet extremely insightful account of how to actually make this work in order to hopefully be of use by those who come after me. The data was provided to the University of Oklahoma in raw SEG-D format and for merging SEG-D into a SEG-Y file I direct the reader to Ben Dowdell's (2013) "Importing SEG-D data into ProMAX 3D." Any field in the parameters not listed is assumed to not require explanation as this is meant as a guide and many parameters will change from survey to survey (i.e. frequencies to process, time to include, maximum offset, etc.). For this process I used JavaSeis tools for data input, output and basic processes, but for the SRME I used the ProMAX processes. I include a PowerPoint guide with images as well as notes for each step along with this thesis on a CD. In the event the CD has become damaged or otherwise lost please contact Dr. Marfurt for another location of the file or my most current contact information if I don't reply by OU email.

I begin with the raw shot gathers that have the geometry applied. Through conversation with those present on acquisition and double checked with some back of the envelope math I discovered that the recording began 100 ms before the shot was fired. This must be removed prior to SRME as it ruins any periodicity of the multiple within the data. To remove the 100 ms I applied a static shift to the data. This is easily performed in ProMAX through the "Header Statics"

process where I added a -100 bulk shift static to the NA_STAT or “Portion of static not applied.” SRME also requires the direct arrive to be muted which can be easily picked on just a few shots and extrapolated based on offset for the others as the direct arrival is consistent with the water velocity and depth of source and receiver remaining relatively constant. I also applied a bandpass filter with corner frequencies of 8-15-80-100 to eliminate the low frequency ocean swell noise.

In or to perform SRME in ProMAX you need to have a rough velocity model. Although SRME is a completely data driven process and requires no prior knowledge or derived information the regularization that interpolates near and far traces does require a velocity model. This can be a 1D model and can be defined in the SRME regularization, but being that I already had a 3D velocity model picked to form the brute stack I decided to use it. Considering that the depth of water does typically vary I recommend that a velocity model be picked. The brute velocity model was picked on a 2.5 km grid. For guidance on velocity picking I again direct the reader to Ben Dowdell’s (2013) thesis in his “Pearsonia Processing” PowerPoint guide.

The final preparation to making 2D SRME work on 3D data is to separate the data by streamer to make it appear as 2D. I did this by redefining the CABLE_ID number and using it as a secondary sorting, but you could use channel as the secondary sort and only bring in the channels of the individual streamer. SRME requires shot gathers so make sure to maintain a shot gather sorting. The first SRME process is “SRME Regularization” the input should be

the shot gather single streamer data. In the parameters I used an offset increment equal to my receiver increment (12.5 m); it is recommended that you always use an offset increment equal to or less than the acquisition parameters. The only problem is when you use an increment less you will have to interleave the data differently than how I present it here in later steps. I chose a maximum offset of 2700 m to encompass all possible offsets and the brute velocity model was used.

After regularization is the “SRME Macro” process. This process is the most important and lengthy as creates the predicted multiples. In this you can processes multiple lines which is good as we have a sudo 2D dataset and SRME needs to be able to recognize when the line has changes and shots no longer correlate to a similar position. To separate these I used the “Sail Line Number.” Now the “flip shot direction” caused me a fair amount of debate as the help documentation says to flip the shot direction if “the order of the shots [is] equivalent to the source pushing the cable.” Well to me that could mean that the data is organized in an odd fashion perhaps decreasing offset or it could mean that the shot number is increasing toward the direction of the receivers. My data was organized such that the source number always increased to the NW but I know that the boat is sometimes traveling SE. So if one were looking at the data by increasing shot and the boat was actually traveling SE then the next shot would look as if it “pushed” the receivers to the NW. I decided to say “yes” to flipping the shot direction on the lines where the boat was traveling SE, this required me to separate the survey up some more but was a simple matter of

looking at the observer logs to determine sail direction then sorting the data as such. I came to this conclusion after running multiple tests and although there was very little difference I did see significant changes in the final result where the slope of the seafloor was changing. For the last parameter of input shot/receiver spacing ratio I chose 2:1 as my shots are every 25 m and my receivers every 12.5 m. The only other parameter that should be noted when using the macro is the “Trace header file name.” This is the name of a temporary file that is created to make the macro result. The thing to note here is that if you are running multiple SRME Macro’s at the same time then each one should have a different Trace Header file name.

With the SRME Macro result written out, the next step is to un-regularize the data. Using the Javaseis tools, as I did, for data input (I did not use the JavaSeis SRME tools) the first step is to combine the original data with the Macro results using a “JavaSeis Data Combine” with the setting to interleave traces. The first data in should be of the original data with the Macro result in the data combine. Following that should be the “SRME Un-Regularization. The un-regularization should use the same velocity model as the regularization did. The output will be the original data followed by the predicted multiples for the offsets present and will be organized such that all the original data (D) is first increasing by offset, then the predicted multiples (N) increasing by offset. If for some reason your data output is not in DDD….NNN format like this do not worry there are other options in the later steps that can allow for you to continue.

The next step is to do the “SRME Matching filter” and “SRME Adaptive Subtraction.” I did the two separate to analyze each result but the two can be run consecutively and not hamper the speed much. For both, you must specify data organization as previously discussed, mine was DDD…NNN. In the Matching filter the parameters to note are the “start time” which I chose to be just before the first reflection and the “Mute noise above start time” which I chose to be “yes,” when I chose “no” a low frequency noise came out in the areas above the first reflection. The “Adjustment velocity” is the adjustment for the start time with offset and was chosen to be the velocity of water (1500 m/s). The “Window length” and “Filter length” were determined heuristically to be 400 ms and 40 ms respectively.

The adaptive subtraction is the final step of SRME and has some of the most confusing parameters. The beginning of this and the most frustrating to discover is the options for “Output option.” Under output option ProMAX gives “Signal,” “Noise,” and “both.” Well Signal is your final output signal with multiples removed and noise is the actual noise removed, but both is not both your signal and noise! Instead it is your original input data with the multiples present and the noise removed! This left me in the testing stage for a very long time because every time I would look at the panel I thought was signal it would look exactly the same even though the noise removed panel showed multiples removed! Do not fall for their dirty tricks; hopefully this will be fixed in the future versions of ProMAX. The Temporal window length and Filter length were determined by trial and error. The spatial averaging size is meant to represent the diameter of a

circle that averages the reflections of the surrounding traces. I found that if I set this to zero little noise was removed and it was sporadic, but with a little spatial averaging the noise removed began to appear more like actual multiple reflections being removed. The “maximum filter coefficient” represents the coefficient which the subtraction can multiple the amplitude of the multiple by in order to remove the entire multiple in the case that the matching filter was not sufficient. The key here is that you do not want to make it too large as you may begin to remove actual geologic reflections. Here, I used 2.0 and found that it may have been very slightly too harsh in initial stacks but did not adversely affect the final PSTM volume.

While this ends the SRME portion you will need to put all your data back together. For me I had four pieces, a set of NW sailing data and SE sailing data, each with streamer 1 and streamer 2. I used the data input and data combine to first put the streamers back together and then the entire survey, this time by “interleaving frames.” Make sure to check your data has been recombined properly and that all channels are present for each shot. With that you have successfully completed 2D SRME on a 3D dataset. I hope it has proven helpful and has saved you from extreme frustration; unfortunately, I am sure that you will still encounter some as ProMAX will change and every data set is different.